ENGINEERING NEW HOLE EXTRACTION MATERIALS FOR LEAD SULFIDE COLLOIDAL QUANTUM DOT PHOTOVOLTAICS

by
Eric Ran Rong

A thesis submitted to Johns Hopkins University in conformity
with the requirements for the degree of Master of Science in Engineering

Baltimore, Maryland
May, 2021

Abstract

Lead Sulfide (PbS) Colloidal Quantum Dots (CQDs) are of interest for photovoltaic (PV) applications due to their low-cost, size-tunable, and solution-processable nature. They efficiently absorb infrared light, which is a major component of the sun's spectrum, and have a direct bandgap. Their low-temperature materials synthesis and facile thin-film fabrication processes allow for scalable manufacturing and flexible substrate applications, such as for building-integrated PV and wearable electronics. Thus, they exhibit potential to expand the adoption of solar energy technology.

However, the efficiency of PbS CQD-based PV is limited in part due to poor carrier mobility in the standard hole transport layer (HTL) in the devices: ethanedithiol-passivated PbS CQD thin films (PbS-EDT). We therefore sought alternate strategies and materials to augment or replace the hole transport layer for improved performance. This thesis investigates the nature of these shortcomings, identifies material characteristics that hamper solar cell performance, proposes materials which address these challenges, and demonstrates improved performance after integration.

This thesis is organized into two sections. The first section describes infusion of elemental sulfur into the PbS-EDT hole transport layer. Based on Solar Capacitance Simulations, we uncovered significant photogeneration occurring in the HTL, which is nonideal behavior that demonstrates the need for better hole mobility, electron mobility, and doping density in this layer. We developed a method of evaporating sulfur atoms onto a PbS-EDT HTL to improve these electronic properties.

The second section describes the deposition of a solution of an exfoliated 2D transition metal dichalcogenide, tungsten diselenide (WSe_2), to enhance the hole transport layer. With insights gained from the study described in the first section, we utilized WSe_2 in our solution-processed device fabrication to augment the PbS-EDT HTL.

Together, this thesis unveils insights, strategies, and methods of engineering novel hole transport layers through a coherent study of materials development.

Thesis Readers

Dr. Susanna M. Thon (Primary Advisor)
Associate Professor
Department of Electrical and Computer Engineering
Johns Hopkins University

Dedicated to my parents, Joann Liu and Charles Rong,
whose love, support, and guidance have been indispensable
in my educational and personal development.

Acknowledgements

First, I would like to acknowledge my wonderful advisor, Dr. Susanna M. Thon. Through her years of thoughtful mentorship, I have grown tremendously as a student, researcher, and intellectual. The rigorous yet supportive research environment she crafted in her group made it a safe environment to learn and grow, which was tremendously important for these formative years of my research career. Her willingness to share her deep understanding of so many scientific concepts used in our work was both inspiring and conducive to learning. I have thoroughly enjoyed learning and working in her research group, and I appreciate all the thought that made such a constructive experience possible.

I would also like to acknowledge my fellow group members in the Nanoenergy Lab, all of whom I have learned greatly from. Their approachability and kindness have made it a great experience to conduct research with and alongside them, and I am always glad to talk with them about any topic, research or non-research related. In particular, I would like to acknowledge Arlene Chiu, who has served as my primary mentor on the hole transport materials project. She has been a pleasure to learn from and work with, and I've learned that we make a great team in tackling all sorts of research problems.

Next, I would like to acknowledge my parents, Dr. Joann Liu and Dr. Charles Rong, who have had an immense impact on my development as a student, as a researcher, and as a person. Their guidance and support have allowed me to carve an independent path for myself, and have helped find my way in times of difficulty.

Much of who I am is attributed to their nurturing influence. This thesis is dedicated to them.

I also would like to acknowledge all my professors, teachers, and mentors who have helped shape my mind through all my years of education. Their lessons and guidance have helped me retain facts, ideas, concepts, and methodologies, but more importantly, they have taught me how to learn. They fuel the fire for learning that I've maintained throughout my life, and that I will always continue to feed.

I would like to acknowledge all my friends that have helped me grow as a person, and have contributed in large part to my education through group study sessions during late nights in the library, the ECE department lounge, and over Zoom. In particular, I would like to acknowledge Yuzuka Karube for providing insightful ideas during thought-provoking discussions that have helped me in my research.

Finally, I would like to acknowledge the funding sources that have made all my work possible, in particular from the National Science Foundation (DMR-1807342).

Contents

Abstract ii

Dedication iv

Acknowledgements v

Contents vii

List of Tables ix

List of Figures x

Chapter 1 Introduction 1

1.1 Introduction to Colloidal Quantum Dots 1

1.2 Synthesis of Colloidal Quantum Dots 2

1.3 Colloidal Quantum Dot Films 2

1.4 Impact of Colloidal Quantum Dot Solar Technology 3

1.5 Motivation for This Work 4

Chapter 2 Chalcogenide-Enhanced Hole Transport Materials to Overcome Carrier Transport Limitations in Colloidal Quantum Dot Solar Cells 5

2.1 Sulfur-Infused Hole Transport Materials to Overcome Performance-Limiting Transport in Colloidal Quantum Dot Solar Cells 5

2.1.1 Introduction and Background . . . 6
2.1.2 SCAPS Calculations of Hole Transport Properties . . . 8
2.1.3 Experimental Methods and Results . . . 11
2.1.4 Conclusions and Future Outlook . . . 17
2.2 New Chalcogenide-Based Hole Transport Materials for Colloidal Quantum Dot Photovoltaics . . . 18
2.2.1 Introduction . . . 18
2.2.2 Experiments and Results . . . 21
2.2.2.1 SCAPS Simulations . . . 21
2.2.2.2 Transfer Matrix Method Calculations . . . 23
2.2.2.3 Energy Band Alignment . . . 25
2.2.2.4 Characterization . . . 25
2.2.3 Conclusion . . . 26

Chapter 3 Conclusions . . . **28**

References . . . **29**

Appendix IExperimental Details and Supplementary Figures . . . **33**
A Experimental Details . . . 33
A.1 PbS CQD Synthesis . . . 33
A.2 Device Fabrication and Sulfur Infusion . . . 34
A.3 Current Density-Voltage Characterization . . . 35
A.4 Space-Charge-Limited Current (SCLC) Measurements . . . 35
A.5 Capacitance-Voltage (Cap-V) Measurements . . . 36
A.6 Ultraviolet Photoelectron Spectroscopy (UPS) . . . 36
B Supplementary Figures . . . 37

List of Tables

2-I Summary of CQD Solar Cell Performance with sulfur infused hole transport layers 14

2-II SCAPS results for the impact of absorbing layer thickness and HTL electron mobility on solar cell efficiency. 23

2-III Summary of experimental CQD solar cell performance with and without WSe_2 in the HTL. 27

I-I SCAPS simulation parameters, measured and from the literature for sulfur infused hole transport layers 37

List of Figures

Figure 1-1 Lead Sulfide Colloidal Quantum Dot solar cell structure 3

Figure 2-1 SCAPS simulation results for sulfur infused hole transport layers 7

Figure 2-2 Schematic of the sulfur-infused hole transport layer fabrication process 12

Figure 2-3 Current density-voltage, Cap-V, doping density, and mobility results for sulfur infused hole transport layers 13

Figure 2-4 Band diagram for a PbS CQD solar cell with a sulfur infused hole transport layer 15

Figure 2-5 Structure of solar cells with and without WSe_2 20

Figure 2-6 SCAPS results for varying hole and electron mobility with WSe_2 in the hole transport layer 22

Figure 2-7 Transfer Matrix Method calculations with WSe_2 in the hole transport layer 24

Figure 2-8 Process of ultrasonically exfoliating bulk WSe_2 into a mono to few-layer solution in ethanol 26

Figure I-1 Full SCAPS simulation results for varying the electron mobility of the hole transport layer 38

Figure I-2 Full SCAPS simulation results for varying the valence band edge energy of the hole transport layer 39

Figure I-3 Transfer matrix method calculations 40

Figure I-4 UPS spectra for sulfur infused hole transport layers 41

Figure I-5 External quantum efficiency of devices with sulfur infused hole transport layers 42

Chapter 1

Introduction

1.1 Introduction to Colloidal Quantum Dots

Lead Sulfide (PbS) colloidal quantum dots (CQDs) are an emerging technology and are of interest for applications in light emission, photodetection, biosensing, and photovoltaics.[1] As a colloidal solution of semiconducting nanocrystals (or "quantum dots") stabilized in solvent, they are compatible with solution processable deposition methods, and can be fabricated into a thin film for use in an optoelectronic device. Their physical properties are thus advantageous for low-cost, scalable fabrication processes, important characteristics that could have a significant impact on expanding the use of photovoltaic technology. Additionally, their optical properties are promising for designing high performance photovoltaic devices. The bandgap of the semiconducting quantum dots, which influences the spectral properties of the absorption of light (important for matching to the sun's spectrum), is determined by the size of each quantum dot.[1]. This relationship is determined by the quantum confinement effect, which allows the tuning of a nanocrystal's bandgap through changing the size of the nanocrystal. Because PbS CQDs are tunable for efficient absorption of infrared light, which comprises a significant portion of the solar spectrum, they can be an improvement over other solution-processed solar materials that do not absorb infrared light efficiently, including lead halide perovskites and organic semiconductors.[2] The

tunability is also promising for tandem and multijunction solar cells, which require stacking materials of different bandgaps to maximize performance.

1.2 Synthesis of Colloidal Quantum Dots

To synthesize colloidal quantum dots, the hot injection method[3] is commonly used. By injecting a sulfur precursor into a heated lead precursor, monomers are formed, which then slowly grow into spherical colloidal nanocrystals.[1] Controlling the size (and thus bandgap) of the quantum dots that form is accomplished through changing the nucleation temperature (temperature of injection) and through controlling the temperature of the post-nucleation growth phase.[1] More specific details about our synthetic process may be found in Appendix I.

These nanocrystals are stably suspended in the solution phase, and are prevented from aggregating because of the surface ligands that cover the surface of the CQDs. Additionally, in the film phase, the choice of ligand can impact the electronic performance of CQD-based devices, as they passivate surface electronic trap states that would otherwise harm efficiency, and they also facilitate inter-dot coupling.[1]

1.3 Colloidal Quantum Dot Films

Creating a film from a CQD solution can be accomplished through solution-processed film deposition techniques, including dip casting, blade casting, spray casting, spin casting, and drop casting.[1] Building a solar cell that incorporates a CQD film requires a series of CQD-based and other layers, depicted in Figure 1-1. The CQD-based material with iodide and bromide ligands serves as the absorbing layer, where light from the sun is absorbed and forms an exciton consisting of an electron-hole pair that quickly dissociates. The electrons are transported through the ZnO nanoparticle (NP) electron transport layer, which blocks holes and carries electrons to the bottom transparent

conductor, fluorine-doped tin oxide (FTO). Similarly, the holes are transported through the ethanedithiol-passivated PbS-CQD (PbS-EDT) hole transport layer, which blocks electrons and transports holes to the gold (Au) top conducting electrode. The resulting current and potential difference can be harnessed to power an external circuit.

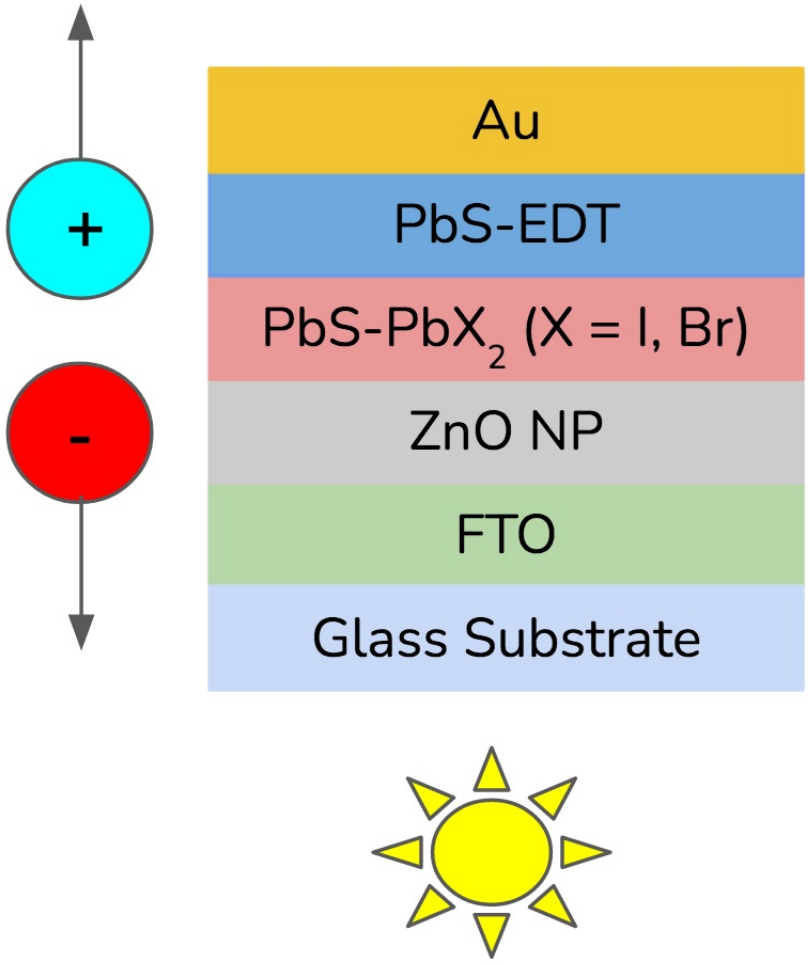

Figure 1-1. Diagram of a Lead Sulfide Colloidal Quantum Dot solar cell structure.

1.4 Impact of Colloidal Quantum Dot Solar Technology

The low cost, solution-phase processability, fabrication scalability,[4, 5] and size tunability through the infrared enable solar cells based on PbS-CQDs to have potential

for new applications of photovoltaics (PV) that are not possible with existing silicon technology, such as building-integrated PV[6, 7] and flexible mobile power sources.[8, 9] However, the state-of-the-art power conversion efficiency (PCE) of PbS-CQD solar cells is 13%,[10] which trails that of silicon, thin-film chalcogenide (CdTe and Cu(In,Ga)Se_2 (CIGS)), and perovskite solar cells, which have all demonstrated PCEs of over 20%.[11] Therefore, more research is needed to further the performance of PbS-CQD solar cells in order for them to be more competitive with existing technologies.

1.5 Motivation for This Work

State-of-the-art Lead Sulfide Colloidal Quantum Dot solar cells make use of a thin layer of ethanedithiol (EDT)-passivated quantum dots through a solid phase ligand exchange process for the hole transport layer.[10] This layer has been shown to exhibit low carrier mobilities and low doping density, and serves as a critical barrier in the improvement of efficiency in PbS-CQD solar cells.[12] As a result, designing new materials to supplant or to supplement the PbS-EDT HTL is of interest for researchers. In this thesis, we investigated addressing this problem through the development of chalcogenide-based materials strategies for enhancing the PbS-EDT based hole transport layer to increase device performance.

Chapter 2

Chalcogenide-Enhanced Hole Transport Materials to Overcome Carrier Transport Limitations in Colloidal Quantum Dot Solar Cells

In this chapter, we investigate the origins of the low performance in the PbS-EDT hole transport materials. We propose two methods of using chalcogenide-based materials to develop new hole transport layers for PbS-CQD photovoltaics. First, we investigate elemental sulfur infusion of the PbS-EDT hole transport layer. Second, we investigate the use of monolayer or few-layer tungsten diselenide (WSe_2) for enhancing or replacing the PbS-EDT hole transport layer.

2.1 Sulfur-Infused Hole Transport Materials to Overcome Performance-Limiting Transport in Colloidal Quantum Dot Solar Cells

2.1.1 Introduction and Background

Semiconductor colloidal quantum dots (CQDs) are nanomaterials of interest for optoelectronic applications because they exhibit size-dependent optical and electronic properties due to quantum confinement effects.[14–17] PbS CQDs are of particular interest for photovoltaics because of their tunable absorption throughout the near-infrared;[3] their earth-abundant materials basis; and their amenability to a variety of solution-processed, scalable fabrication methods,[4, 5] all of which enable their promising applications in multijunction solar cells,[18, 19]) color-tuned devices for building-integrated photovoltaics,[6, 7] and flexible electronics.[8, 9] The field of PbS CQD photovoltaics has achieved power conversion efficiencies (PCEs) of over 13%[10] attributed to improvements in materials,[20, 21] device architectures,[22, 23] and surface ligand engineering.[24, 25] Although advances in efficiency continue apace, the best-performing silicon, thin-film chalcogenide (CdTe and Cu(In,Ga)Se_2 (CIGS)), and perovskite solar cells have surpassed 20% PCE.[11] Therefore, higher efficiencies are needed in CQD solar cells in order for them to be competitive with other technologies.

The solar cell layer structure used in the highest-efficiency PbS CQD solar cells[26] is shown in Figure 2-1c. The absorbing layer consists of oleic acid-capped CQDs that have undergone a solution-phase ligand exchange with PbX_2 (X = Br, I) and ammonium acetate ("PbS-PbX_2" in the diagram). ZnO serves as the n-type electron transport layer (ETL) in CQD solar cells, which effectively blocks hole transport while efficiently transporting electrons through. This material has been studied in depth[27, 28] and is generally considered to have a high doping density up to $10^{18} cm^{-3}$ as well as ideal band alignment with the PbS CQD absorbing materials.[29] The hole transport layer (HTL) is meant to minimize leakage and recombination by facilitating hole transport to, and band alignment with, the deep work function metal top contact, while also blocking electron transport.[30] Current high-performing CQD solar cells use a thin ($< 100nm$) layer of PbS CQDs with solid-state-exchanged ethanedithiol

(EDT) ligands as the p-type HTL.[10] This material exhibits low carrier mobilities and relatively low doping densities, making it presumably a critical barrier in the highest-performing CQD solar cell devices.[12] Development of the HTL has been more recent and focused on new ligand strategies, which have achieved promising results.[31, 32]

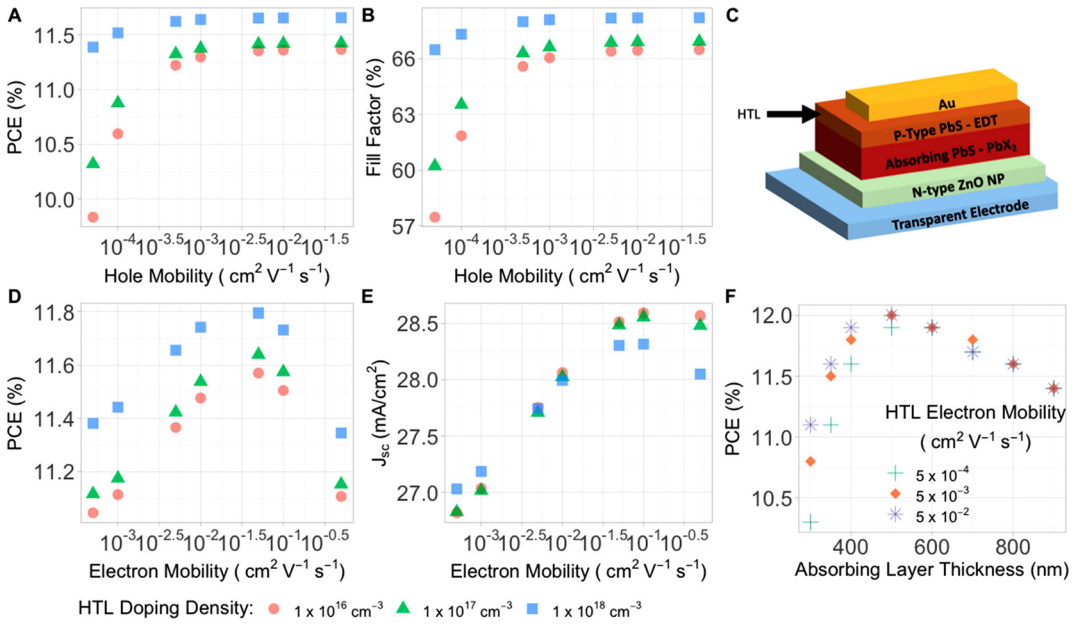

Figure 2-1. SCAPS simulations results: (a and b) PCE and fill factor, respectively, as a function of HTL hole mobility with a constant HTL electron mobility of $5 \times 10^{-3} cm^2 V^{-1} s^{-1}$ and HTL doping densities of 1×10^{16} (red circles), 1×10^{17} (green triangles), and 1×10^{18} (blue squares). (c) Diagram of the CQD solar cell layer structure consisting of a bottom transparent substrate (not shown), a transparent electrode (fluorine-doped tin oxide in this work), a wide bandgap electron-extracting n-type semiconductor (ZnO), an intrinsic bulk absorbing PbS-PbX_2 (X = Br, I) CQD thin film, a thin hole-extracting p-type PbS CQD film treated with ethanedithiol (EDT) ligands, and a top evaporated Au contact. The hole-transporting layer (HTL) is indicated by a black arrow. (d and e) PCE and J_{sc}, respectively, as a function of HTL electron mobility with a constant hole mobility of $5 \times 10^{-2} cm^2 V^{-1} s^{-1}$. (f) PCE as a function of absorbing layer thickness for HTL electron mobilities of $5 \times 10^{-4} cm^2 V^{-1} s^{-1}$ (green crosses), $5 \times 10^{-3} cm^2 V^{-1} s^{-1}$ (orange diamonds), and $5 \times 10^{-2} cm^2 V^{-1} s^{-1}$ (purple stars).

In this work, we elucidate the impact of the HTL electronic properties, including carrier mobilities, doping density, and energy band levels, on device efficiency using one-dimensional Solar Cell Capacitance Simulator (SCAPS) calculations.[33] Using the

insights gained from this study, we introduce elemental sulfur as a means of performing stoichiometric control of the HTL. Our new HTL material shows increased p-type character[34] and improved CQD photovoltaic efficiencies via sulfur surface passivation, which facilitates higher electron mobilities for photogenerated electrons within the HTL. We use capacitance-voltage (Cap-V) measurements to obtain doping densities, space-charge-limited current (SCLC) measurements to acquire carrier mobilities, and current density-voltage (J-V) measurements under simulated solar illumination to measure solar cell device performance parameters. By increasing the doping density and electron mobility of our HTLs through stoichiometry tuning, we achieved a clear improvement in device performance, from a maximum of 9.3% to 10.4% power conversion efficiency. The improvement of the HTL that we demonstrate could have immediate applications in flexible, wearable, building-integrated, and multijunction photovoltaics. Our study also provides insights that can be used to further improve the performance of CQD solar cells, including the necessity of improving transport in the absorbing layer so that it can be made thick enough to prevent photogeneration in the HTL.

2.1.2 SCAPS Calculations of Hole Transport Properties

In order to determine the limiting factors in the performance of CQD solar cells, we undertook a variational computational study of critical parameters associated with the HTL. Specifically, we used SCAPS to study the effects of the HTL doping density and both electron and hole mobility, as well as the band alignment between the absorbing layer and the HTL, on the performance of the CQD solar cell. SCAPS is a one-dimensional solar cell simulator that takes parameters such as carrier mobilities, doping densities, and recombination center densities as inputs and uses the drift-diffusion and Poisson's equations to calculate J-V characteristics and energy band diagrams.[33] We used materials parameters based on literature values for CQD solar

cells detailed in Table I-I [35–37] and layer thicknesses of 350 nm for the PbS-PbX_2 absorbing layer and 60 nm for the PbS-EDT HTL layer, based on our own thickness optimization studies. We varied the doping density in the HTL from 10^16 to $10^18 cm^{-3}$, the electron mobility from 5×10^{-4} to $5 \times 10^{-1} cm^2 V^{-1} s^{-1}$, and the hole mobility from 5×10^{-5} to $5 \times 10^{-2} cm^2 V^{-1} s^{-1}$. These parameter ranges represented reasonable values based on our own results and results from the literature[38–41] for the HTL. The full results for all parameter combinations are detailed in Figure I-1.

Figure 2-1 shows the simulation results for the doping density, hole mobility, and electron mobility of the HTL. We note that, in general, the device PCE increases with an increase in doping density, electron mobility, and hole mobility of the HTL. In Figure 2-1a,b, the PCE and fill factor (FF) are plotted as a function of HTL hole mobility for different values of the HTL doping density, with the electron mobility set to our experimental value of $5 \times 10^{-3} cm^2 V^{-1} s^{-1}$. The observed increases in PCE with both increasing hole mobility and doping density can largely be attributed to increases in device FF, which generally tracks with the expected decrease in resistivity associated with higher doping densities. This effect saturates, however, beyond a hole mobility of approximately $5 \times 10^{-4} cm^2 V^{-1} s^{-1}$; increasing the hole mobility in the HTL beyond this value has a minimal impact on the performance of the solar cell for all values of the doping density. We note that most currently used HTLs in CQD solar cells are reported to have hole mobilities greater than $5 \times 10^{-4} cm^2 V^{-1} s^{-1}$, as will be discussed in the context of our experimental results below.

More surprisingly, we also observe an increase in PCE with increasing electron mobility of the HTL from 5×10^{-4} to $5 \times 10^{-1} cm^2 V^{-1} s^{-1}$, as seen in Figure 2-1d, with the hole mobility set to our experimental value of $5 \times 10^{-2} cm^2 V^{-1} s^{-1}$. This can be mostly attributed to an increase in the short-circuit current (J_{SC}), as seen in Figure 2-1e. We also observe that when the electron mobility becomes greater than the hole mobility used in the simulations ($5 \times 10^{-1} cm^2 V^{-1} s^{-1}$), the performance of the solar

cell begins to decline.

The improved device performance associated with increasing electron mobility in the HTL is an unexpected result. The electron mobility in the HTL should have a negligible impact on device performance under ideal circumstances, given that the function of the HTL is to block electrons and transport holes only. We hypothesize that this could mean that significant photogeneration happens in the HTL such that this layer also plays a non-negligible role in electron transport. Similar photogeneration observations have previously been attributed to optical interference effects at the top contact interface.[42]

We tested this hypothesis by running a series of simulations in which we varied the thickness of the PbS-PbX_2 absorbing layer to see if there was a point at which the electron mobility of the HTL no longer played a significant role in device performance. The results are shown in Figure 2-1f. We varied the electron mobility in the HTL from 5×10^{-4} to $5 \times 10^{-}2 cm^2 V^{-1} s^{-1}$ and the absorbing layer thickness from 300 to $900nm$. At our experimental value of the absorbing layer thickness, $350nm$, increasing the electron mobility in the HTL has a strong positive effect on PCE. However, as the absorbing layer thickness increases, the impact of electron mobility decreases and becomes negligible at absorbing layer thicknesses of larger than approximately $500nm$, where the device performances peaks. We further confirmed our hypothesis that significant photogeneration is predicted to occur in the HTL by using transfer-matrix method calculations[43] to quantify the spatial electric field profile in our device. We found that 10.2% of the optical total absorption occurs in the HTL, as can be seen in Figure I-3. This roughly matches with the predicted improvement in J_{SC} due to improvements in electron mobility in the HTL (Figure 2-1e).

We also performed band structure simulations to determine the optimal alignment between the absorbing layer and the HTL. We varied the valence band edge energy difference between the HTL and the absorbing layer from zero to $0.4eV$, with the HTL

valence band edge assumed to be shallower than the absorbing layer edge. The results are shown in Figure I-2. We found that for the standard (PbS-EDT) HTL (doping density of $2.54 \times 10^{17} cm^{-3}$, hole mobility of $5.58 \times 10^{-2} cm^2 V^{-1} s^{-1}$, and electron mobility of $1.05 \times 10^{-3} cm^2 V^{-1} s^{-1}$), the optimal valence band energy difference is approximately $0.15eV$. For an optimized HTL (doping density of $1.10 \times 10^{18} cm^{-3}$, hole mobility of $5.23 \times 10^{-2} cm^2 V^{-1} s^{-1}$, and electron mobility of $1.65 \times 10^{-2} cm^2 V^{-1} s^{-1}$), the optimal valence band energy difference is approximately $0.23eV$. Full SCAPS results for the band structures of different device configurations are shown in Figure 2-4b.

To summarize the results of our SCAPS simulations, we found that, given the current properties of the absorbing layer, a good HTL needs a doping density of at least $10^{18} cm^{-3}$, an electron mobility greater than $5 \times 10^{-2} cm^2 V^{-1} s^{-1}$, a hole mobility greater than $5 \times 10^{-4} cm^2 V^{-1} s^{-1}$, and a valence band edge difference between the absorbing layer and the HTL of approximately $0.23eV$. We therefore sought to design and fabricate a new material that was compatible with standard CQD solar cell fabrication methods while fulfilling the above requirements. This led us to explore elemental sulfur infusion of the PbS-EDT materials, which has been previously shown to improve carrier mobilities and increase p-type doping density in CQD field effect transistors.[44] We hypothesized that introducing elemental sulfur into the PbS-EDT materials would allow us to control the stoichiometry of the CQDs that comprise the HTL, reducing the density of surface traps that limit carrier mobilities while fine-tuning the band edge energies and Fermi level.

2.1.3 Experimental Methods and Results

We used electron beam evaporation to infuse elemental sulfur into the standard PbS-EDT HTL, keeping all other device fabrication procedures the same as in previous reports[24, 45, 46] and as described in Experimental Methods in Appendix I. The

experimental procedure is illustrated schematically in Figure 2-2a. We tested effective sulfur thicknesses of 1, 3, 6, 9, and 15Å, as monitored using the built-in quartz crystal oscillator in our electron beam evaporator. We estimate that an effective evaporation thickness of 15Å of sulfur corresponds to roughly 30 atoms of sulfur per nanocrystal on average, using the following assumptions: The HTL CQD films have a density of roughly $1.8 \times 10^{14} nanocrystals/cm^2$, assuming a face-centered cubic packing profile derived from TEM images, and a layer thickness of approximately $60nm$; the density of the cubic close-packed structure of sulfur yields about $3.13 \times 10^{22} atoms/cm^3$.

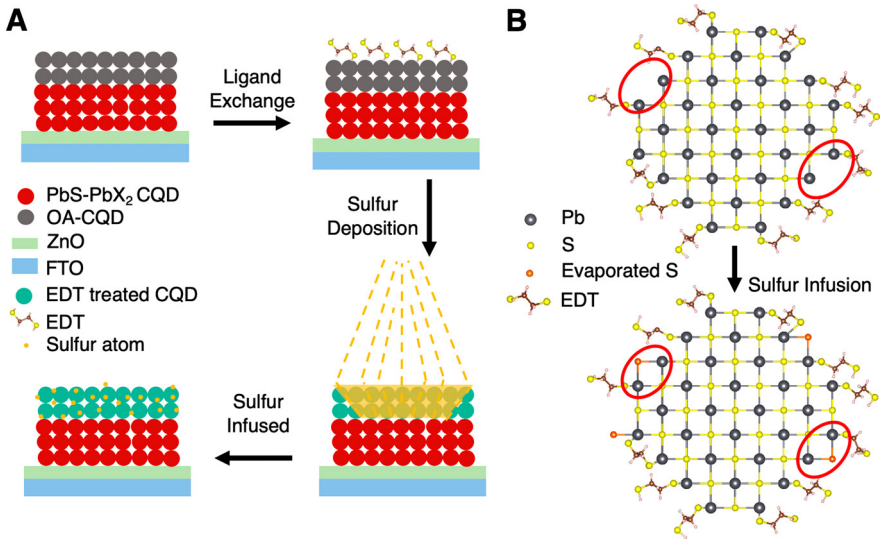

Figure 2-2. (a) Schematic of the sulfur-infused hole transport layer fabrication process. A PbS CQD film with oleic acid ligands (upper left) undergoes a solid-state exchange to EDT ligands (upper right). The film is then infused with elemental sulfur via electron beam evaporation (lower right), resulting in a stoichiometry-tuned film (lower left). (b) A truncated cross-sectional schematic of a single PbS CQD with EDT ligands only (top) and after sulfur infusion (bottom). Empty Pb-bonding sites are partially filled with sulfur atoms, as indicated by the red outlines.

We measured current-density-voltage characteristics under simulated AM1.5G solar illumination of our solar cells with different HTLs to extract the relevant solar cell device parameters. From the results shown in Table 2-I, we see that there is a gradual increase in CQD solar cell PCE that plateaus with an increasing amount of sulfur, up to 15Å. Comparing the best performing sulfur-infused solar cell, with 15Å

of sulfur, to our control device with no sulfur infusion, we see an absolute increase of 1% in the PCE, from 9.32% to 10.35%, a relative increase of 11% (Figure 2-3a), and an absolute average increase of 1.5% from 7.51% to 9.00%. Consistent with our SCAPS simulation results, the increase in the PCE is due to increases in both the fill factor and the short-circuit current, while the open-circuit voltage is relatively unaffected by sulfur-infusion of the HTL.

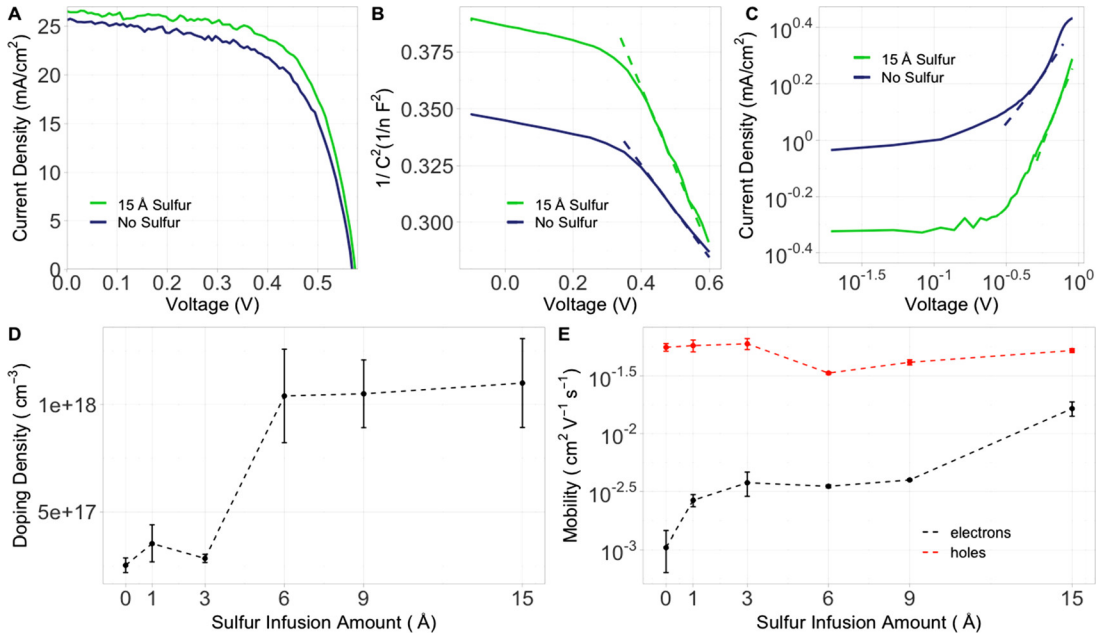

Figure 2-3. (a) Current density-voltage plots of the best performing control HTL device (purple) and a 15Å sulfur HTL device (green). (b) Cap-V measurement results of a control HTL device (purple) and a 15Å sulfur HTL device (green) and the fit lines used to extract the doping densities (dashed). (c) Current-voltage log plot of an electron-transport SCLC structure control HTL device (purple) and a 15Å sulfur HTL device (green), with the SCLC region, used to calculate the electron mobility, indicated by dashed lines. (d) Average doping density in the HTL extracted from Cap-V measurements as a function of HTL sulfur infusion amount. (e) Hole mobility (red) and electron mobility (black) extracted from SCLC measurements as a function of HTL sulfur infusion amount.

To verify that the increase in PCE was primarily a result of an increase in the doping density and electron mobility of the HTL, we used Cap-V measurements and SCLC measurements, respectively, to characterize our different HTLs. Using Cap-V measurements, we extracted an average doping density of $2.5 \times 10^{17} cm^{-3}$ for the PbS-EDT HTL in our control devices without sulfur addition and an average doping

density of $1.1 \times 10^{18} cm^{-3}$ for the 15Å sulfur-infused HTL. We found that there was a notable increase in the doping density as the amount of sulfur in the HTL was increased from 3 to 6Å (Figure 2-3b,d), which correlated with a similar trend in the PCE. The largest PCE increase, from 9.2% to 9.8% for the best performing solar cells of each type and from 7.8% to 8.7% for the average of each type of cell, occurred as the amount of sulfur in the HTL was increased from 3 to 6Å.

sulfur	PCE [%], best (average)	V_{OC} [V], best (average)	J_{SC} [mA cm^{-2}], best (average)	fill factor, best (average)
none	9.32 (7.51 ± 0.98)	0.57 (0.56 ± 0.01)	25.61 (21.32 ± 2.50)	0.61 (0.61 ± 0.01)
1 Å	9.16 (7.72 ± 0.95)	0.58 (0.57 ± 0.01)	24.97 (21.63 ± 2.65)	0.62 (0.61 ± 0.01)
3 Å	9.22 (7.79 ± 1.2)	0.58 (0.57 ± 0.01)	23.79 (21.22 ± 2.71)	0.64 (0.61 ± 0.03)
6 Å	9.80 (8.67 ± 0.39)	0.57 (0.57 ± 0.00)	25.72 (23.84 ± 1.00)	0.65 (0.62 ± 0.02)
9 Å	9.97 (9.04 ± 0.74)	0.58 (0.58 ± 0.01)	26.21 (24.07 ± 1.84)	0.64 (0.63 ± 0.01)
15 Å	10.35 (9.00 ± 0.62)	0.58 (0.57 ± 0.00)	26.51 (24.17 ± 1.47)	0.65 (0.63 ± 0.01)

[1] Measured over a total of 246 solar cells; $30 - 59$ for each row.

Table 2-I. Summary of CQD Solar Cell Performance [1] with sulfur infused hole transport layers

We performed ultraviolet photoelectron spectroscopy (UPS) measurements (Figure I-4) to determine the location of the valence band edges of the HTL and absorbing layer materials and to verify any band structure shifts from the sulfur-infusion-induced modification of the CQD surface structure, as illustrated in Figure 2-2b. We found that the control PbS-EDT HTL had a valence band edge that was approximately $0.07eV$ shallower than that of the absorbing CQD layer. The difference for the 15 Å sulfur-infused HTL and the absorbing CQD layer increased to about $0.12eV$ (Figure

2-4a). We note that both of these energy differences are approximately $0.1eV$ smaller than the ideal band alignment predicted by our SCAPS simulations for their relative doping densities (Figure I-2).

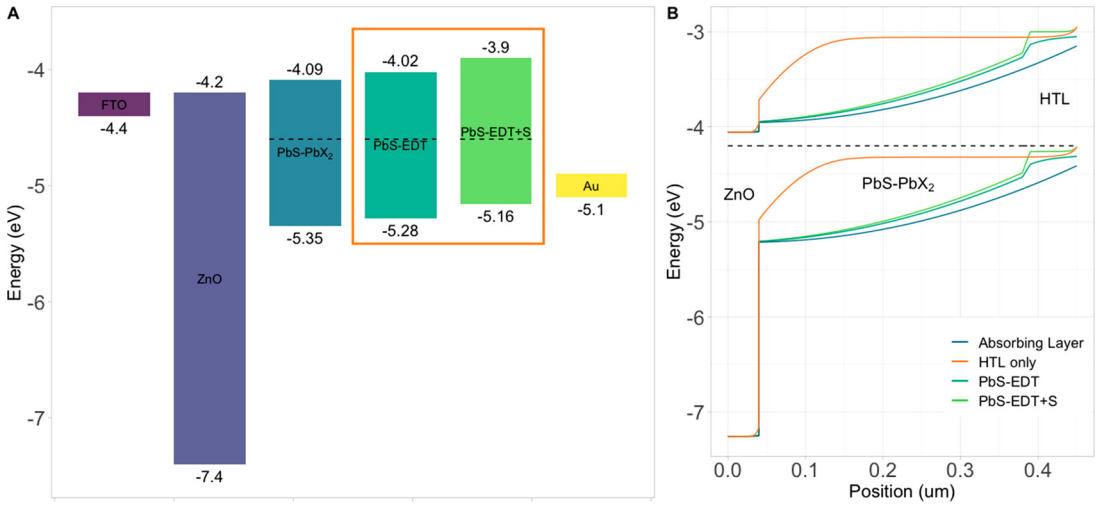

Figure 2-4. (a) Band diagram for a PbS CQD solar cell, with the HTL layer alternatives highlighted by the orange box. Band edge positions are taken from the literature (FTO,[47] ZnO[37], and Au[48]) and extracted from UPS and UV-vis-NIR spectrophotometric absorption measurements (PbS-PbX_2, PbS-EDT, and PbS-EDT+S). (b) SCAPS simulated band diagrams at equilibrium for different solar cell devices: the full structure shown in Figure 2-1c with a sulfur-infused HTL (light green), the full structure with a nonsulfur-infused HTL (dark green), a device with an absorbing layer but no HTL (blue), and a device with a nonsulfur-infused HTL but no absorbing layer (orange). The Fermi level is indicated by the black dashed line, and regions corresponding to the different layers of the solar cell are indicated.

We used space-charge-limited current (SCLC) measurements to measure the carrier mobilities in our HTL[49, 50] (Figure 2-3c,e). The SCLC method uses a device architecture with the semiconductor material of interest inserted between one charge injection contact and one injection-blocking electrode to ensure that current in the device is due to only one carrier type.[38, 41] Dark current-voltage curves are measured, and carrier mobility is extracted by fitting the SCLC region, where there is a quadratic relationship between the applied current and voltage.

In this regime, charges tend to accumulate in the region between the electrodes, and the electric field, and thus the current, is dependent on only the carrier mobility, which

can be extracted using the Mott-Gurney Law. For hole mobility measurements, we used an ITO bottom contact, a poly(3,4-ethylenedioxythiophene) polystyrene sulfonate (PEDOT:PSS) layer, the semiconducting test layer (either the HTL or absorbing PbS CQD layer), and a Au top contact. The hole mobility results for a range of sulfur infusion conditions are shown in Figure 2-3e. We found that sulfur infusion had a minimal impact on hole mobility, with all results on the order of $10^{-2} cm^2 V^{-1} s^{-1}$, 2 orders of magnitude greater than the threshold required for PCE saturation of $5 \times 10^{-4} cm^2 V^{-1} s^{-1}$, which was calculated assuming the control experimental values of the electron mobility and doping density.

For electron mobility measurements, our device architecture consisted of a fluorine-doped tin oxide (FTO) bottom contact, a ZnO anode, the semiconducting test layer (either the HTL or absorbing PbS CQD layer), and a Au top contact. We measured a gradual increase in the electron mobility as the amount of sulfur in the HTL was increased, totaling an order of magnitude increase from an average of $1.05 \times 10^{-3} cm^2 V^{-1} s^{-1}1$ to $1.65 \times 10^{-2} cm^2 V^{-1} s^{-1}$, for the control HTL device with no sulfur and the device with 15Å of sulfur in the HTL, respectively. We posit that the increase in effective electron mobility could arise from sulfur passivation of the surface trap states of the EDT-ligated CQDs, as has been previously observed.[25, 51, 52]

We also performed external quantum efficiency (EQE) measurements (Figure I-5), which confirmed our experimental results, even after several months of device aging. There is an overall improvement in the current across all wavelengths with the addition of sulfur to the HTL, which is likely a result of the higher doping density in the HTL and consequent larger charge-extracting drift field. There is an additional current enhancement at the exciton peak wavelength, which could be attributed to better collection of longer-wavelength photons, which are more likely to be absorbed near the back of the device, because of the improved HTL electron mobility.

Our experimental results confirmed the predictions from the SCAPS simulations.

The primary effect of the sulfur infusion was to increase the doping density and electron mobility in the HTL compared to the control PbS-EDT HTL. The increase in both of these properties correlated with an increase in solar cell PCE, primarily through increases in the short-circuit current and fill factor, as expected.

2.1.4 Conclusions and Future Outlook

To summarize, we set out to understand the requirements of a good HTL for CQD solar cells and to develop a new strategy to implement these requirements. Using 1D SCAPS simulations, we studied the effects of the HTL doping density, carrier mobility, and relative band edge locations on device performance. We found that the hole mobilities in current HTL materials are predicted to be sufficient for high efficiency and are not currently the limiting factor in performance. Instead, we found that increasing the doping density in the HTL by an order of magnitude should have a significant effect on PCE, and counterintuitively, low electron mobility in the HTL was limiting performance because of a significant amount of photogeneration occurring in the HTL. We then developed a new strategy to address these limitations: sulfur infusion of the traditional PbS-EDT HTL to increase the p-type character by shifting the stoichiometry of the film and improving the electron mobility through passivation of surface electron trap states. We demonstrated that our new HTL behaved as predicted, achieving an average absolute increase of 1.5% in the PCE over solar cells with the PbS-EDT HTL.

This work points to new directions for further improvements in CQD solar cell PCE through engineering of both the HTL and CQD absorbing layer properties. Specifically, carrier transport in the CQD absorbing layer should be improved so that this layer can be made thick enough such that significant photogeneration does not need to occur in the HTL.

2.2 New Chalcogenide-Based Hole Transport Materials for Colloidal Quantum Dot Photovoltaics

Two-dimensional transition metal dichalcogenides (TMDs) are a family of graphene-like materials that exhibit promising electrical and optical properties for electronic and optical devices.[53] The bulk TMD crystals are easily exfoliated into monolayers by breaking the Van der Waals forces between monolayers, which do not possess dangling bonds that would harm device performance.[54] By tuning the composition of the material, the number of layers, and the strain of the crystals, the electronic properties can be modified.[54] Here, we propose and investigate the use of WSe_2, a TMD, for use in enhancing or replacing the PbS-EDT hole transport material in colloidal quantum dot solar cells.

2.2.1 Introduction

Lead Sulfide (PbS) colloidal quantum dots (CQDs) are advantageous for photovoltaic (PV) applications due to their size-tunable optical properties, their absorption in the infrared, and their inexpensive nature[3]. Their low-temperature material synthesis and solution-phase processability allow for facile thin-film fabrication techniques in scalable and flexible applications of solar energy technology, such as for building-integrated PV and wearable electronics, enabling new frontiers in the widespread adoption of renewable energy. Current state-of-the-art PbS CQD solar cell architectures, shown in Fig. 2-5a, are comprised of a fluorine-doped tin oxide (FTO) transparent conductive oxide contact, a zinc oxide (ZnO) nanoparticle-based electron transport layer (ETL),

an absorbing layer of oleic acid-capped PbS CQDs that undergo a solution-phase ligand exchange with PbX_2 (X = Br, I) and ammonium acetate, a hole transport layer (HTL) of oleic acid-capped PbS CQDs that undergo a solid-phase ligand exchange with ethanedithiol (PbS-EDT), and a gold top contact[26].

However, PbS CQD-based solar cells exhibit limitations in efficiency, one source of which originates in the HTL[13]. The function of the HTL is to block electron transport, facilitate hole transport, prevent recombination, and to align the band structure of the absorbing layer with the deep work function metal top contact[13]. The highest efficiency PbS CQD solar cells utilize a thin (approximately 60 nm) PbS-EDT layer as the HTL[31], which exhibits low carrier mobility[12]. New methods of enhancing the transport characteristics of the HTL are thus desired to improve the performance of PbS CQD-based solar cells.

In this work, we use one-dimensional Solar Cell Capacitance Simulations (SCAPS-1D)[33] to determine the impact of the HTL electron mobility and hole mobility on device efficiency and Transfer Matrix Method (TMM) calculations to determine the absorption and generation profile of a solar cell. We then propose using chalcogenide-based materials to enhance the HTL carrier mobility and thus overall solar cell performance. In particular, we deposit a near-monolayer of tungsten diselenide (WSe_2), a 2D transition metal dichalcogenide (TMD), to act as the HTL. We characterized these solar devices with current density-voltage (JV) measurements to obtain solar cell performance metrics. The insights into the limitations of the PbS-EDT HTL and the improvements in the HTL that we demonstrate could be applied to developing new HTL materials or enhancing performance in CQD-based solar cells and other optoelectronic devices.

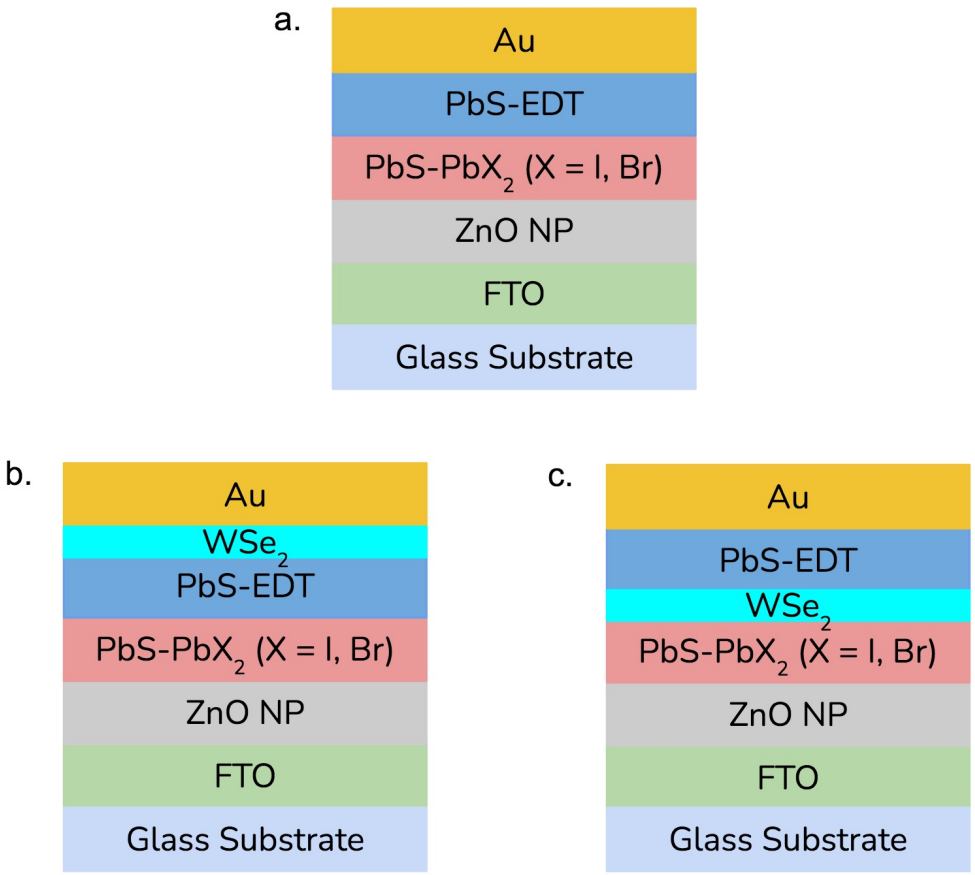

Figure 2-5. (a) Structure of a state-of-the-art PbS CQD solar cell, with a PbS-EDT HTL. (b) Structure of a PbS CQD solar cell with an HTL that is augmented by a layer of WSe_2 between the PbS-EDT and the gold electrode. (c) Structure of a PbS CQD solar cell with an HTL that is augmented by a layer of WSe_2 between the absorbing layer and the PbS-EDT.

2.2.2 Experiments and Results

2.2.2.1 SCAPS Simulations

To better understand the factors inhibiting HTL performance and to determine the properties of a material that will improve it, we used SCAPS simulations to specifically look at the impact of electron mobility and hole mobility. For a structure with a 350 nm thick PbS-PbX_2 absorbing layer and a 60 nm thick PbS-EDT HTL, determined by empirical thickness optimization experiments, we used material parameters based on values from the literature[35–37]. We varied the electron mobility from 5 x 10^{-4} to 5 x 10^{-1} cm^2 V^{-1} s^{-1} and hole mobility from 5 x 10^{-5} to 5 x 10^{-2} cm^2 V^{-1} s^{-1}, which we determined based on values reported in the literature for PbS-EDT films[13].

Fig. 2-6 shows simulation results for the effect of HTL hole and electron mobility on power conversion efficiency (PCE) of the full solar cell. The electron mobility is kept constant at 5 x 10^{-3} cm^2 V^{-1} s^{-1}, for the hole mobility calculations (blue asterisks), and the hole mobility is kept constant at 5 x 10^{-2} cm^2 V^{-1} s^{-1} for the electron mobility calculations (orange crosses). We found that increasing both hole and electron mobility increased efficiency, so we were interested in developing a HTL material that exhibits both higher electron and hole mobility than PbS-EDT.

The increased efficiency due to increased hole mobility was expected, as higher hole mobility should facilitate more effective hole transfer through the HTL. However, the existence of a region where increasing the electron mobility in the HTL resulted in increased PCE was less intuitive, since the HTL typically functions to block electron transfer. Past work has theorized that significant photogeneration can occur in the HTL. This could explain the effect, since mobile carriers generated in the HTL would benefit from effective electron transfer through this layer to be collected as photocurrent[56]. We tested this theory by varying the thickness of the PbS-PbX_2 absorbing layer from $300 - 900$nm, as well as the HTL electron mobility from 5 x

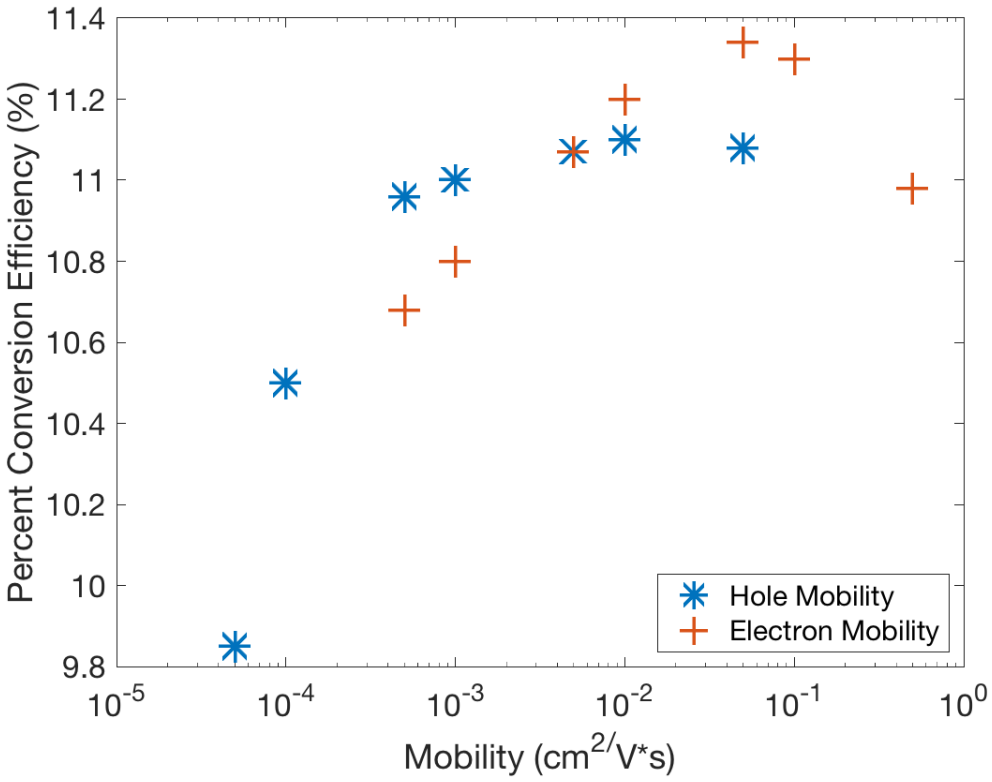

Figure 2-6. SCAPS results for the effect of varying HTL mobility on solar cell efficiency. PCE when varying hole mobility (with constant electron mobility of 5 x 10^{-3} cm^2 V^{-1} s^{-1}) is given by the blue asterisks, and PCE when varying electron mobility (with constant hole mobility of 5 x 10^{-2} cm^2 V^{-1} s^{-1}) is given by the orange crosses.

10^{-4} to 5 x 10^{-2} cm^2 V^{-1} s^{-1} in simulations, and seeing if there was a point at which increased electron mobility ceased to improve the PCE. The results in Table 2-II show that the device performance peaks at a PbS-PbX_2 thickness of around 500 nm, and that with absorbing layers thicker than 500 nm, increasing the HTL electron mobility ceased to impact overall device PCE. After that point, absorption in the HTL is negligible, and, therefore, high electron mobility does not significantly impact charge transfer. This explains why, for a sufficiently thick absorbing layer, electron mobility increases in the HTL do not impact PCE, which confirms our hypothesis.

Table 2-II. SCAPS results for the impact of absorbing layer thickness and HTL electron mobility on solar cell efficiency.

	Absorbing Layer Thickness (nm)							
HTL Electron Mobility (cm^2/Vs)	300	350	400	500	600	700	800	900
5e-4	10.3	11.1	11.6	11.9	11.9	11.7	11.6	11.4
5e-3	10.8	11.5	11.8	12.0	11.9	11.8	11.6	11.4
5e-2	11.1	11.6	11.9	12.0	11.9	11.7	11.6	11.4

2.2.2.2 Transfer Matrix Method Calculations

To further confirm that significant photogeneration occurs in the HTL, we performed TMM calculations to quantify the absorption and generation in the standard PbS-EDT HTL solar cell[43]. The results in Fig. 2-7 demonstrate that 10.2% of overall total optical absorption occurs in the HTL, with larger percentages at longer wavelengths. This shows that significant photogeneration happens in the HTL, further confirming the results of our SCAPS simulations.

Because the fraction of light absorbed in the HTL contributes significantly to the overall power generation in the cell, we sought to enhance the performance of the PbS-EDT layer by increasing its hole and electron mobilities.

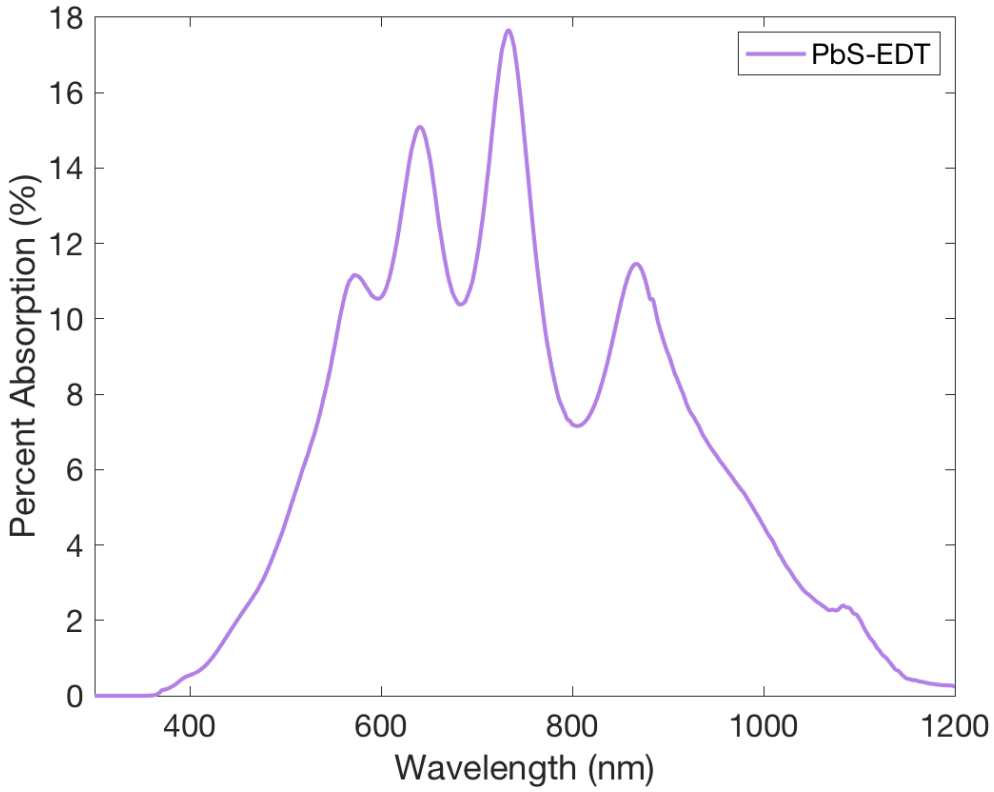

Figure 2-7. Transfer Matrix Method calculations showing the wavelength-dependent absorption by the PbS-EDT HTL as a fraction of total device absorbance.

2.2.2.3 Energy Band Alignment

In addition to carrier mobility, the energy band structure of the HTL plays an important role in device performance. We performed ultraviolet photoelectron spectroscopy (UPS) measurements to determine the valence band edge locations of the absorbing layer and HTL, as well as ultraviolet-visible-near-infrared (UV-Vis-NIR) spectrophotometric measurements to determine the bandgap of each layer. We found that the valence band edge for the PbS-EDT HTL is approximately 0.07 eV shallower than that of the absorbing layer. Our SCAPS simulations indicated that the optimal valence band edge for the HTL should be 0.23 eV shallower than that of the absorbing layer [26]. Based on this, we sought a suitable material with higher hole mobility, electron mobility, p-type character and optimal band alignment.

Monolayer WSe_2 was identified as a promising candidate, with reported hole mobility of 250 cm^2 V^{-1} s^{-1}, electron mobility of 140 cm^2 V^{-1} s^{-1}[54], p-type doping[53], and similar band alignment to PbS-EDT, with valence band edges around -5.28 eV for PbS-EDT and around -5.3 eV for WSe_2[57].

2.2.2.4 Characterization

We fabricated solar cells with the structure described in Section 2.2.1 and Fig. 2-5a. To introduce the WSe_2 into the structure, we used spin-casting to deposit a thin film of WSe_2 from the solution-phase. The solution consists of suspended nanoflakes ranging from approximately one to ten atomic layers in thickness with ethanol as the solvent, which were ultrasonically exfoliated as shown in Fig. 2-8. We fabricated a standard structure with PbS-EDT as the HTL, a structure with a layer of WSe_2 between the absorbing layer and the PbS-EDT layer (Fig. 2-5c.), and a structure with a layer of WSe_2 between the PbS-EDT and Au layer (Fig. 2-5b.). Additionally, we fabricated structures with the same spin deposition process as the WSe_2 solutions, replacing the WSe_2 solution with pure ethanol, to determine if any impacts to performance result

from the ethanol or from the WSe_2.

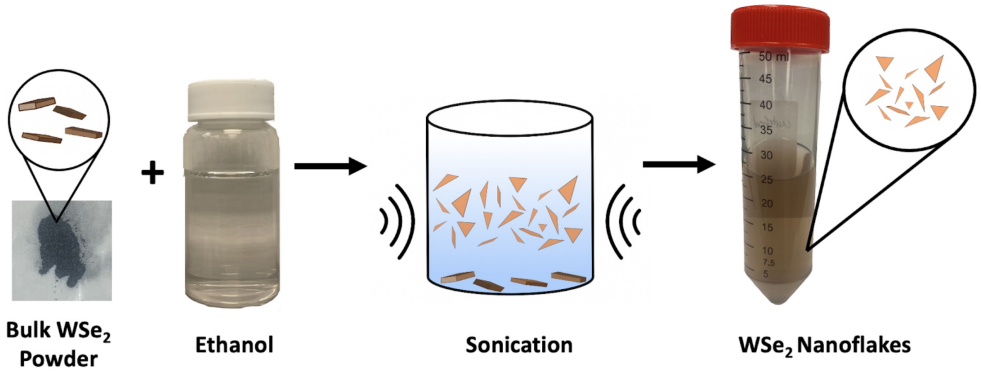

Figure 2-8. Process of ultrasonically exfoliating bulk WSe_2 into a mono to few-layer solution in ethanol. Reprinted with permission from Ref. [58].

We then characterized these devices using JV measurements under simulated solar illumination to determine solar cell efficiency and related figures of merit. We obtained the results in Table 2-III, with 16 and 47 devices tested per architecture. When comparing the WSe_2 devices to their pure ethanol counterparts, we notice an improvement in best device performance of the devices containing WSe_2, meaning that the presence of ethanol does not account for the entire performance increase. We also see that both structures containing WSe_2 perform better than the control in the best device, demonstrating that augmenting the PbS-EDT with a WSe_2 layer improves solar cell performance, most noticeably through improvements in the fill factor. The slightly higher overall performance of the PbS-EDT/WSe_2 structure may be explained by better band alignment with the absorbing layer.

2.2.3 Conclusion

We performed SCAPS-1D simulations to identify the performance-limiting factors in CQD solar cell HTLs. We discovered that, paradoxically, increasing the electron mobility in the HTL correspondingly increased the efficiency of the overall solar cell, even though the HTL theoretically serves primarily to block electrons. We hypothesized that this could mean that significant photogeneration occurs in the HTL,

Table 2-III. Summary of experimental CQD solar cell performance with and without WSe_2 in the HTL.

Structure	**PCE [%] Best (Average)**	**Voc [V] Best (Average)**	**Jsc [mA/cm^2] Best (Average)**	**FF [%] Best (Average)**
PbS-EDT	8.37 (7.3±0.56)	0.58 (0.58)	28.24 (24.97±1.61)	51.0 (50.0±1.6)
PbS-EDT/Ethanol	9.42 (8.08±1.31)	0.55 (0.53±0.05)	29.15 (26.53±1.91)	59.0 (57.0±3.73)
PbS-EDT/WSe_2	9.72 (7.95±1.37)	0.58 (0.56±0.06)	27.84 (25.76±2.03)	60.0 (54.0±5.3)
Ethanol/PbS-EDT	8.69 (7.69±0.72)	0.54 (0.53±0.03)	29.18 (26.32±1.80)	55.0 (55.0±0.53)
WSe_2/PbS-EDT	9.20 (7.92±0.98)	0.56 (0.55±0.02)	29.67 (26.31±1.81)	60.0 (54.3±4.4)

so we investigated the influence of increasing the absorbing layer thickness to reduce the amount of HTL photogeneration. We found that increasing the HTL electron mobility ceases to improve the overall PCE when the absorbing layer thickness is greater than 500 nm. We confirmed these results with TMM calculations, which determined that approximately ten percent of the total device photogeneration occurs in the HTL, motivating the need for better hole and electron mobilities in the HTL. We hypothesized that augmenting the PbS-EDT HTL with a thin WSe_2 layer could improve hole and electron mobility while also having similarly compatible band alignment, thereby increasing solar efficiency. We found that our strategy increases the PCE of PbS CQD-based solar cells by 1.35% in the best device. Future work will involve developing HTLs consisting entirely of WSe_2 which should further improve PbS CQD solar cell PCEs.

Chapter 3

Conclusions

This thesis focuses on engineering chalcogenide-based hole transport materials for colloidal quantum dot solar cells. Through simulations, experimentation, and characterization techniques, we have discovered factors influencing bottlenecks in CQD solar cell efficiency, and demonstrated promising methods for designing new materials to combat such issues, which have been shown to improve figures of merit for solar cell performance. The two specific approaches described here, stoichiometric tuning of the traditional HTL film via elemental sulfur infusion, and thin film deposition of a tungsten diselenide nanoflake solution, both show promise. Work still remains before PbS-CQD based solar cells to have the necessary efficiency and longevity to be developed into commercially viable solar panels. However, with continued research on each of these topics, PbS-CQDs remain a highly promising and viable material for furthering the solar energy revolution and reducing our society's dependence on non-renewable energy sources.

References

1. Cheng, Y., Arinze, E. S., Palmquist, N. & Thon, S. M. Advancing Colloidal Quantum Dot Photovoltaic Technology. *Nanophotonics* **5,** 31–54 (2016).
2. Zheng, S., Chen, J., Johansson, E. M. & Zhang, X. PbS Colloidal Quantum Dot Inks for Infrared Solar Cells. *iScience* **23,** 101753 (2020).
3. Hines, M. A. & Scholes, G. D. Colloidal PbS Nanocrystals with Size-Tunable Near-Infrared Emission: Observation of Post-Synthesis Self-Narrowing of the Particle Size Distribution. *Adv. Mater.* **15,** 1844 (2003).
4. Kramer, I. J. *et al.* Efficient Spray-Coated Colloidal Quantum Dot Solar Cells. *Adv. Mater.* **27,** 116 (2015).
5. Loiudice, A. *et al.* Room-Temperature Treatments for All-Inorganic Nanocrystal Solar Cell Devices. *Thin Solid Films* **560,** 44 (2014).
6. Arinze, E. S. *et al.* Color-Tuned and Transparent Colloidal Quantum Dot Solar Cells via Optimized Multilayer Interference. *Opt. Express* **25,** A101 (2017).
7. Hestnes, A. G. Building Integration of Solar Energy Systems. *Sol. Energy* **67,** 181 (1999).
8. He, J. *et al.* Flexible Lead Sulfide Colloidal Quantum Dot Photodetector Using Pencil Graphite Electrodes on Paper Substrates. *J. Alloys Compd.* **596,** 73 (2014).
9. Kramer, I. J., Moreno-Bautista, G., Minor, J. C., Kopilovic, D. & Sargent, E. H. Colloidal Quantum Dot Solar Cells on Curved and Flexible Substrates. *Appl. Phys. Lett.* **105,** 163902 (2014).
10. Choi, M.-J. *et al.* Cascade Surface Modification of Colloidal Quantum Dot Inks Enables Efficient Bulk Homojunction Photovoltaics. *Nat. Commun.* **11,** 103 (2020).
11. Green, M. A. *et al.* Solar Cell Efficiency Tables (Version 55). *Prog. Photovoltaics* **28,** 3 (2020).
12. Lin, Y., Ung, G., Qiu, B., Qian, G. & Thon, S. M. Integrated Concentrators for Scalable High-Power Generation from Colloidal Quantum Dot Solar Cells. *ACS Appl. Energy Mater.* **1,** 2592 (2018).
13. Chiu, A. *et al.* Sulfur-Infused Hole Transport Materials to Overcome Performance-Limiting Transport in Colloidal Quantum Dot Solar Cells. *ACS Energy Letters* **5,** 2897–2904 (2020).
14. Bawendi, M. G., Steigerwald, M. L. & Brus, L. E. The Quantum Mechanics of Larger Semiconductor Clusters ("Quantum Dots"). *Annu. Rev. Phys. Chem.* **41,** 477 (1990).

15. Song, J. H. & Jeong, S. Colloidal Quantum Dot Based Solar Cells: From Materials to Devices. *Nano Converg.* **4,** 21 (2017).

16. Shirasaki, Y., Supran, G. J., Bawendi, M. G. & Bulović, V. Emergence of Colloidal Quantum-Dot Light-Emitting Technologies. *Nat. Photonics* **7,** 13 (2013).

17. Yang, Z. *et al.* Recent Advances in Quantum Dot-Based Light-Emitting Devices: Challenges and Possible Solutions. *Mater. Today* **24,** 69 (2019).

18. Wang, X. *et al.* Tandem Colloidal Quantum Dot Solar Cells Employing a Graded Recombination Layer. *Nat. Photonics* **5,** 480 (2011).

19. Manekkathodi, A. *et al.* Solution-Processed Perovskite-Colloidal Quantum Dot Tandem Solar Cells for Photon Collection beyond 1000 Nm. *J. Mater. Chem. A* **7,** 26020 (2019).

20. Zhang, J., Gao, J., Miller, E. M., Luther, J. M. & Beard, M. C. Diffusion-Controlled Synthesis of PbS and PbSe Quantum Dots with in Situ Halide Passivation for Quantum Dot Solar Cells. *ACS Nano* **8,** 614 (2014).

21. Yuan, M. *et al.* High-Performance Quantum-Dot Solids via Elemental Sulfur Synthesis. *Adv. Mater.* **26,** 3513 (2014).

22. Maraghechi, P. *et al.* The Donor–Supply Electrode Enhances Performance in Colloidal Quantum Dot Solar Cells. *ACS Nano* **7,** 6111 (2013).

23. Chuang, C.-H. M., Brown, P. R., Bulović, V. & Bawendi, M. G. Improved Performance and Stability in Quantum Dot Solar Cells through Band Alignment Engineering. *Nat. Mater.* **13,** 796 (2014).

24. Ip, A. H. *et al.* Hybrid Passivated Colloidal Quantum Dot Solids. *Nat. Nanotechnol.* **7,** 577 (2012).

25. Tang, J. *et al.* Colloidal-Quantum-Dot Photovoltaics Using Atomic-Ligand Passivation. *Nat. Mater.* **10,** 765 (2011).

26. Liu, M. *et al.* Hybrid Organic–Inorganic Inks Flatten the Energy Landscape in Colloidal Quantum Dot Solids. *Nat. Mater.* **16,** 258 (2017).

27. Wang, H. *et al.* Enhanced Carrier Transport Distance in Colloidal PbS Quantum-Dot-Based Solar Cells Using ZnO Nanowires. *J. Phys. Chem. C* **119,** 27265 (2015).

28. Lan, X. *et al.* Passivation Using Molecular Halides Increases Quantum Dot Solar Cell Performance. *Adv. Mater.* **28,** 299 (2016).

29. Willis, S. M., Cheng, C., Assender, H. E. & Watt, A. A. R. The Transitional Heterojunction Behavior of PbS/ZnO Colloidal Quantum Dot Solar Cells. *Nano Lett.* **12,** 1522 (2012).

30. Litvin, A. P. *et al.* Colloidal Quantum Dots for Optoelectronics. *J. Mater. Chem. A* **5,** 13252 (2017).

31. Biondi, M. *et al.* A Chemically Orthogonal Hole Transport Layer for Efficient Colloidal Quantum Dot Solar Cells. *Adv. Mater.* **32,** 1906199 (2020).

32. Teh, Z. L. *et al.* Enhanced Power Conversion Efficiency via Hybrid Ligand Exchange Treatment of P-Type PbS Quantum Dots. *ACS Appl. Mater. Interfaces* **12,** 22751 (2020).

33. Burgelman, M., Nollet, P. & Degrave, S. Modelling Polycrystalline Semiconductor Solar Cells. *Thin Solid Films* **361–362,** 527 (2000).

34. Oh, S. J. *et al.* Stoichiometric Control of Lead Chalcogenide Nanocrystal Solids to Enhance Their Electronic and Optoelectronic Device Performance. *ACS Nano* **7,** 2413 (2013).

35. Ray, J. *et al.* PbS-ZnO Solar Cell: A Numerical Simulation. *J. Nano- Electron. Phys.* **9,** 03041–1 (2017).

36. Sharma, A., Yadav, R. S. & Pandey, B. P. Performance Analysis of PbS Colloidal Quantum Dot Solar Cell at Different Absorption Coefficient. *J. Energy Environ. Sustain.* **7,** 32 (2019).

37. Zhang, X. & Johansson, E. M. J. Reduction of Charge Recombination in PbS Colloidal Quantum Dot Solar Cells at the Quantum Dot/ZnO Interface by Inserting a MgZnO Buffer Layer. *J. Mater. Chem. A* **5,** 303 (2017).

38. Cho, Y. *et al.* Balancing Charge Carrier Transport in a Quantum Dot P–N Junction toward Hysteresis-Free High-Performance Solar Cells. *ACS Energy Lett.* **3,** 1036 (2018).

39. Huang, S. *et al. Improving hole extraction for PbS quantum dot solar cells* en. in. [Online; accessed 2020-06-11] (IEEE, Waikoloa Village, HI, June 2018), 2756–2758.

40. Gu, M. *et al.* Stable PbS Quantum Dot Ink for Efficient Solar Cells by Solution-Phase Ligand Engineering. *J. Mater. Chem. A* **7,** 15951 (2019).

41. Speirs, M. J. *et al.* Temperature Dependent Behaviour of Lead Sulfide Quantum Dot Solar Cells and Films. *Energy Environ. Sci.* **9,** 2916 (2016).

42. Ouellette, O. *et al.* Spatial Collection in Colloidal Quantum Dot Solar Cells. *Adv. Funct. Mater.* **30,** 1908200 (2020).

43. Burkhard, G. F., Hoke, E. T. & McGehee, M. D. Accounting for Interference, Scattering, and Electrode Absorption to Make Accurate Internal Quantum Efficiency Measurements in Organic and Other Thin Solar Cells. *Adv. Mater.* **22,** 3293 (2010).

44. Balazs, D. M. *et al.* Stoichiometric Control of the Density of States in PbS Colloidal Quantum Dot Solids. *Sci. Adv.* **3,** eaao1558 (2017).

45. Liu, L. *et al.* Ligand and Solvent Effects on Hole Transport in Colloidal Quantum Dot Assemblies for Electronic Devices. *ACS Appl. Nano Mater.* **1,** 5217 (2018).

46. Xu, J. *et al.* 2D Matrix Engineering for Homogeneous Quantum Dot Coupling in Photovoltaic Solids. *Nat. Nanotechnol.* **13,** 456 (2018).

47. Helander, M. G., Greiner, M. T., Wang, Z. B. & Tang, W. M. Work Function of Fluorine Doped Tin Oxide. *J. Vac. Sci. Technol., A* **29,** 011019 (2011).

48. Sachtler, W. M. H., Dorgelo, G. J. H. & Holscher, A. A. The Work Function of Gold. *Surf. Sci.* **5,** 221 (1966).

49. Kwan Kim, J., Hoon Song, J., Choi, H., Jae Baik, S. & Jeong, S. Space Charge Limited Conduction in Ultrathin PbS Quantum Dot Solid Diodes. *J. Appl. Phys.* **115,** 054302 (2014).

50. Rath, A. K., Lasanta, T., Bernechea, M., Diedenhofen, S. L. & Konstantatos, G. Determination of Carrier Lifetime and Mobility in Colloidal Quantum Dot Films via Impedance Spectroscopy. *Appl. Phys. Lett.* **104,** 063504 (2014).

51. Jeong, K. S. *et al.* Enhanced Mobility-Lifetime Products in PbS Colloidal Quantum Dot Photovoltaics. *ACS Nano* **6,** 89 (2012).

52. Barkhouse, D. A. R., Pattantyus-Abraham, A. G., Levina, L. & Sargent, E. H. Thiols Passivate Recombination Centers in Colloidal Quantum Dots Leading to Enhanced Photovoltaic Device Efficiency. *ACS Nano* **2,** 2356 (2008).

53. Zhao, P. *et al.* Air Stable p-Doping of WSe_2 by Covalent Functionalization. *ACS Nano* **8,** 10808–10814 (2014).

54. Liu, W., Cao, W., Kang, J. & Banerjee, K. High-Performance Field-Effect-Transistors on Monolayer WSe_2. *ECS Trans.* **58,** 281–285 (2013).

55. Rong, E. *et al. New Chalcogenide-Based Hole Transport Materials for Colloidal Quantum Dot Photovoltaics* en. in (IEEE, Miami-Fort Lauderdale, FL, June 2021).

56. Chiu, A. *et al. New Hole Transport Materials via Stoichiometry-Tuning for Colloidal Quantum Dot Photovoltaics* en. in (IEEE, Calgary, AB, June 2020), 1096–1097.

57. Liu, Y., Stradins, P. & Wei, S. Van der Waals Metal-Semiconductor Junction: Weak Fermi Level Pinning Enables Effective Tuning of Schottky Barrier. *Sci. Adv.* **2** (2016).

58. Chiu, A. *Engineering Colloidal Quantum-Confined Nanomaterials for Multi-junction Solar Cell Applications* Thesis Proposal. 2021.

59. Zhao, Y.-B. *et al.* Accelerated Solution-Phase Exchanges Minimize Defects in Colloidal Quantum Dot Solids. *Nano Energy* **63,** 103876 (2019).

60. Aqoma, H. *et al.* High-Efficiency Photovoltaic Devices using Trap-Controlled Quantum-Dot Ink prepared via Phase-Transfer Exchange. *Advanced Materials* **29,** 1605756 (2017).

Appendix I

Experimental Details and Supplementary Figures

A Experimental Details

A.1 PbS CQD Synthesis

The PbS CQDs were synthesized using previously reported methods.[24] Lead(II) oxide ($0.45g$), 1-octadecene ($3mL$), and oleic acid ($1.5mL$) were mixed in a three-neck flask and degassed under vacuum for 16 hours at $95°C$ using a Schlenk line. After the degassing and the formation of the lead oleate complex, the solution became clear, and the environment was purged with nitrogen gas. $15mL$ of 1-octadecene (ODE) was added and the temperature was set to $120°C$. When the solution reached the desired temperature, $210mL$ of bis(trimethylsilyl)sulfide ($(TMS)_2S$) dissolved in $10mL$ of ODE was quickly injected into the lead oleate solution, which turned dark brown due to the PbS nanocrystal nucleation. The heating source was then removed, and the solution was allowed to cool to $36°C$. After $36°C$ was reached, $20mL$ of acetone

was added, and the mixture was stirred under nitrogen for 2 minutes. An additional $30mL$ of acetone was added, and the solution was centrifuged at 3500 RPM for 5 mins to isolate the CQDs. The isolated CQDs were dispersed in toluene, and the isolation procedure was performed two more times. The CQD in toluene solution was then washed in a nitrogen glovebox using methanol, and after drying, the oleic-acid capped PbS CQDs were dispersed in octane to form a $50mg/mL$ solution.

A.2 Device Fabrication and Sulfur Infusion

Our solar cell device design was based on previous demonstrations. [45] Three layers of ZnO nanoparticles dispersed in chloroform and methanol in a 1 : 1 ratio were spin-cast onto a FTO/glass substrate to form an approximately $200nm$ thick layer.[46] The absorbing PbS CQD film ($350nm$ in thickness) with PbX_2 (X = Br, I) surface passivation[24] was formed by exchanging $4ml$ of $50mg/mL$ oleic acid-capped PbS CQDs in octane with a precursor solution of lead halides (lead iodide and lead bromide) and ammonium acetate in $20mL$ dimethylformamide (DMF).[59] After washing with toluene and octane, the remaining PbX_2-capped CQD solid powder was dissolved in a hybrid-amine solution consisting of n-butylamine (BTA), amylamine, and hexylamine (volume ratio 10 : 3 : 2) at a concentration of $300mg/mL$. The resulting ink was spin-cast and post-annealed at $70°C$ for 10 minutes in a nitrogen rich environment.[46] Two layers of PbS CQDs with ethanedithiol (EDT) ligands, totaling $60nm$, made up the control hole-extracting p-type layer. For each layer, oleic-acid capped PbS CQDs dispersed in octane ($50mg/mL$) were spin-cast and soaked in a 1,2-Ethanedithiol solution ($0.01vol\%$ in acetonitrile) for 15 seconds for the ligand exchange, and then washed 3 times with acetonitrile. Lastly, a $100nm$ gold contact was deposited via electron beam evaporation through a shadow mask to define the device active area. To tune the stoichiometry of the hole transport layer, an electron beam evaporator was used to evaporate varying thicknesses of

elemental sulfur, including 1Å, 3Å, 6Å, 9Å, and 15Å, directly onto the PbS-EDT CQD layer before top contact evaporation. For Cap-V and SCLC electron mobility measurements, a device architecture of FTO/ZnO/PbS-CQDs/Au was used, where the PbS-CQD layer was either PbX_2 (X = Br, I) for absorbing layer only devices, or PbS-EDT with and without additional sulfur for the HTL only devices. For SCLC hole mobility measurements, a device architecture of ITO/PEDOT:PSS/PbS-CQDs/Au was used.[38] Using glass substrates with pre-deposited indium tin oxide (ITO), 3 layers of PEDOT:PSS dispersed in IPA at a 1 : 5 ratio were spin-cast at 2000 rpm for 30 seconds. The remaining layers were prepared as described above.

A.3 Current Density-Voltage Characterization

The current density-voltage (J-V) characteristics of the CQD solar cells were measured through a shadow mask the size of the device area, under simulated AM1.5 illumination set to $100 mW/cm^{-2}$ using a calibrated silicon solar cell. A Keithley 2400 SourceMeter was used to source voltage and measure current.

A.4 Space-Charge-Limited Current (SCLC) Measurements

SCLC measurements of current-voltage in dark conditions under reverse bias were used to extract charge carrier mobilities, using the device configurations described above. J-V plots were fit using the Mott-Gurney Law, equation I.1, where J is the current density, ϵ_0 is the free-space permittivity, ϵ is the dielectric constant of the PbS-CQD film (21.2, from [60]), V is the applied voltage, L is the thickness of the layer and μ is the carrier mobility.

$$J = \frac{9}{8}\epsilon\mu\frac{V^2}{L^3} \tag{I.1}$$

A.5 Capacitance-Voltage (Cap-V) Measurements

Using a Keithley 590 C-V analyzer, we performed capacitance-voltage measurements at $100kHz$ under reverse bias in dark conditions. To extract doping densities in the HTL and absorbing layer, we used FTO/ZnO/HTL/Au and FTO/ZnO/PbX_2 (X = Br, I)/Au device configurations, respectively. We produced Mott-Schottky plots ($1/C^2$ vs. V) and fit the linear region of the plots to extract doping densities using equation I.2, where C is the capacitance, q is the elementary charge, and N_D is the doping density.

$$C^{-2} = \frac{2}{qA^2\epsilon N_D}V \tag{I.2}$$

A.6 Ultraviolet Photoelectron Spectroscopy (UPS)

To study the valence bands, UPS spectra were taken under ultra-high vacuum with a Kratos X-ray Photoelectron Spectrometer - Axis Ultra DLD using the He I line ($21.2eV$) of a helium lamp. The valence band edge energy was calculated by performing a Fermi edge calibration with a clean Au standard and a linear regression on the valence band maximum. We used an Agilent Cary 5000 UV-Vis-NIR spectrophotometer with an integrating sphere insert to measure absorbance spectra of the films to obtain the bandgap energies.

B Supplementary Figures

Parameters	ZnO	$PbS–PbX_2$	HTM
Thickness (nm)	40	350	60
Bandgap (eV)	3.2	1.26	1.26
Electron Affinity (eV)	4.2	4.1	4
Dielectric Permittivity (relative)	8.5	20	20
CB/VB Effective Density of States ($1/cm^3$)	5E19	1E19	1E19
Electron Thermal Velocity (cm/s)	1E7	7E3	7E3
Hole Thermal Velocity (cm/s)	1E7	7E3	1E3
Electron Mobility (cm^2/Vs)	5E-2	1E-3	5E-4 to 5E-1
Hole Mobility (cm^2/Vs)	5E-2	1E-1	5E-5 to 5E-2
Ndonor ($1/cm^3$)	2E18	1E15	1E14
Nacceptor($1/cm^3$)	0	1E15	1E16 to 1E18

Table I-I. SCAPS simulation parameters, measured and from the literature for sulfur infused hole transport layers.[35, 36]

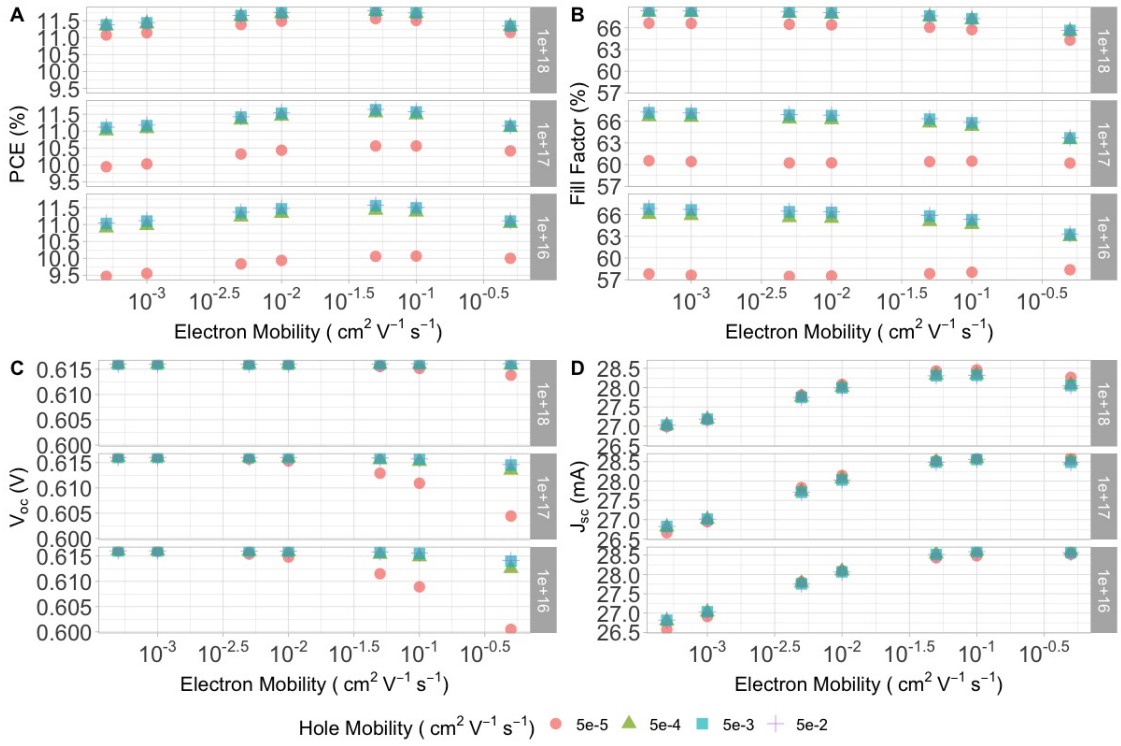

Figure I-1. Full SCAPS simulation results for CQD solar cell performance as a function of electron mobility of the hole transport layer (HTL). The doping density of the HTL is indicated in the grey boxes the right of each plot. Plot symbol type and color denote hole mobility of the HTL as follows: $5E^{-5}cm^2V^{-1}s^{-1}$ = red circles, $5E^{-4}cm^2V^{-1}s^{-1}$ = green triangles, $5E^{-3}cm^2V^{-1}s^{-1}$ = blue squares, $5E^{-2}cm^2V^{-1}s^{-1}$ = purple crosses. a) Power conversion efficiency, b) Fill factor, c) Open-circuit voltage, d) Short-circuit current density.

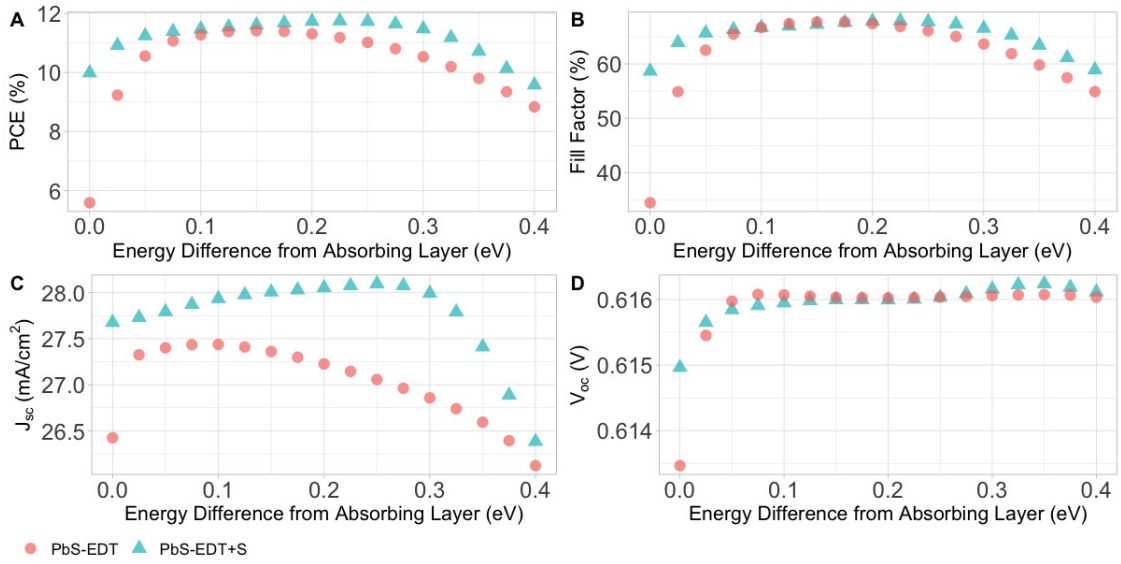

Figure I-2. Full SCAPS simulation results for CQD solar cell performance as a function of HTL valence band edge energy relative to the CQD film absorbing layer valence band edge energy. Results are calculated for carrier mobilities and doping densities corresponding to those measured for the PbS-EDT HTL materials (red circles) and to those measured for the PbS-EDT+S HTL materials (blue triangles). a) Power conversion efficiency, b) Fill factor, c) Short-circuit current density, d) Open-circuit voltage.

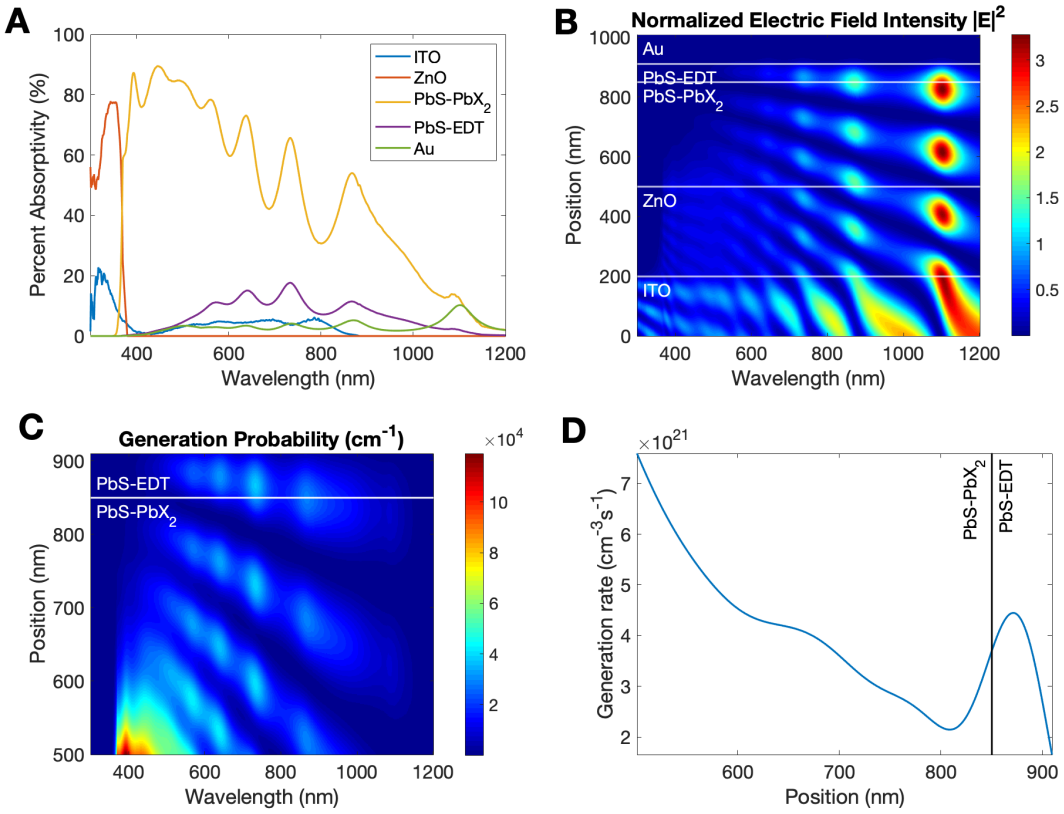

Figure I-3. Transfer-matrix method calculation results for a) percent absorption occurring in each CQD solar cell device layer as a function of wavelength, b) spatial electric field intensity profile, normalized to the excitation source intensity, for the vertical direction (position) in the device as a function of wavelength with individual layers labeled, c) photogeneration probability in the two CQD-based layers as a function of wavelength, and d) total generation rate in the two CQD-based layers.

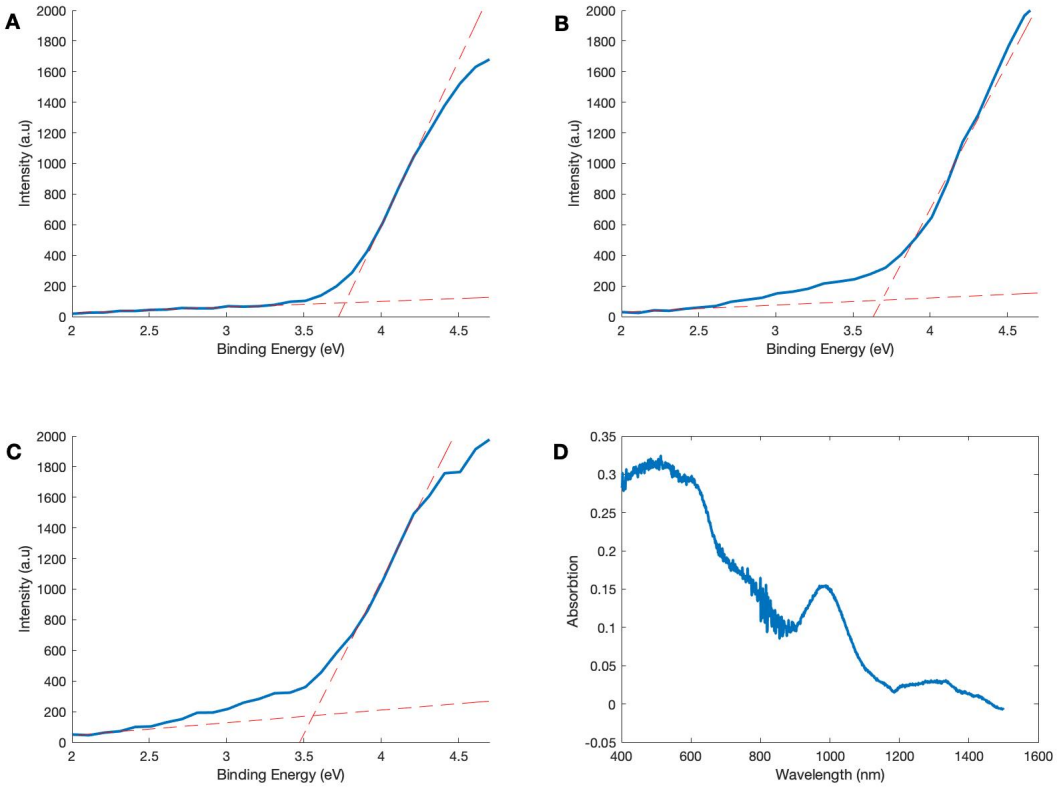

Figure I-4. UPS spectra (blue) with linear fit lines used to extract the valence band edge energies of a) the PbS-PbX_2 CQD film absorbing layer, b) the PbS-EDT control HTL, and c) the PbS-EDT+S HTL with 15Å of sulfur. d) UV-Vis-NIR absorption spectrum of the film-phase PbS-PbX_2 (X = Br, I) absorbing layer.

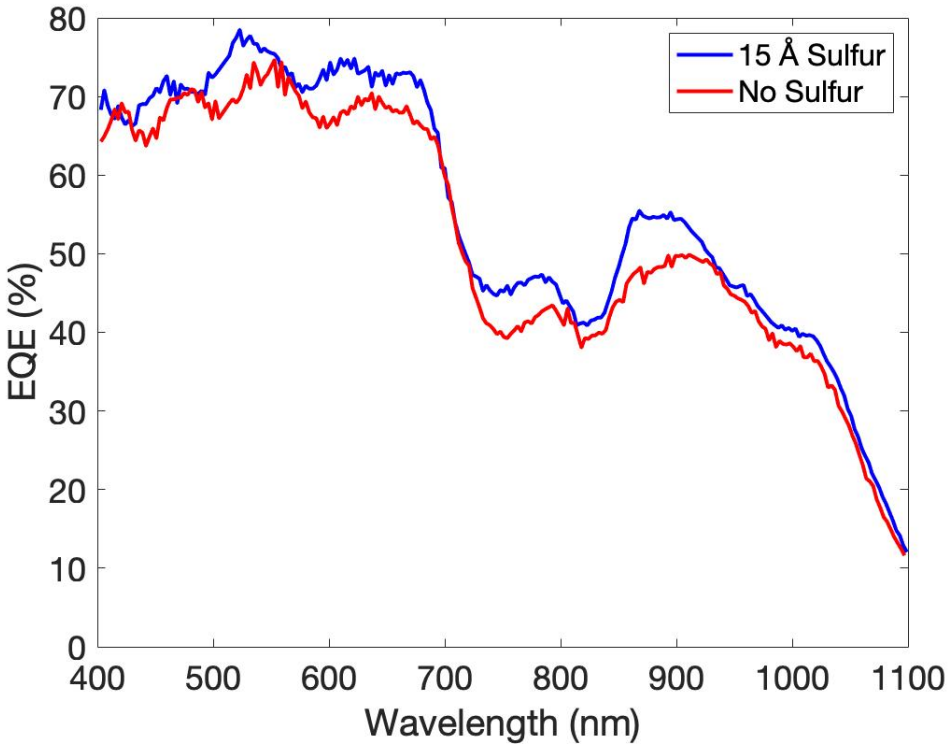

Figure I-5. External quantum efficiency for a CQD solar cell with a sulfur-infused HTL (15Å of sulfur, blue) and a control CQD solar cell (red). Note that these measurements were taken after several months of device aging, and the devices demonstrate slightly lower overall currents than several-day-old devices. However, we expect the spectral trends to be consistent.

Eric Rong

Phone: 202-517-3000 • Email: eric.r.rong@gmail.com • https://orcid.org/0000-0001-8088-1730

Education

Johns Hopkins University, Baltimore, MD **Expected May 2021**

- **Master of Science in Engineering**, Electrical Engineering
  Thesis: Engineering New Hole Extraction Materials for Lead Sulfide Colloidal Quantum Dot Photovoltaics
- **Bachelor of Science**, Electrical Engineering (major), Computer Science (minor).

Relevant Skills

Languages: Java, C++, C, Python, MATLAB, LabVIEW, R, Arduino, VHDL, x86 Assembly, LaTeX
Software: PCB Design, Autodesk Inventor, ArcGIS, SPICE, Cadence Virtuoso, Unix Shell, Git
Coursework: Quantum Mechanics, Semiconductor Physics, Optoelectronics, Photonics, Electromagnetism, Digital Signal Processing, Very Large-Scale Integration, Photovoltaics, Analog and Digital Circuits, Computer Architecture, Data Structures, Machine Learning, Software Engineering, Business, Corporate Strategy

Work and Research Experience

Nanoenergy Lab, Dept. of Electrical & Computer Engineering (ECE) **Spring 2019-present**

- Optimized transparent electrode fabrication for all spray-cast colloidal quantum dot solar cells (CQD SC)
- Simulated and developed two different novel chalcogenide-enhanced hole transport materials in CQD SCs
- Developing techniques for quantum dot coupling with periodic materials for energy generation and storage

Computer System Fundamentals Head Course Assistant, Dept. of Computer Science **Fall 2019-present**

- Led and coordinated 11 course assistants' instructional activities, developed improvements to course material based on feedback and experience, resolved course issues, developed automated grading tests

General Physics II Learning Assistant, Dept. of Physics & Astronomy **Fall 2018-Spring 2019**

- Taught undergraduate students in lecture and section, assisted professors and graduate TAs

Activities

Secretary, Institute of Electrical and Electronics Engineers, JHU Chapter **Fall 2020-present**

- Developed interest-based subgroups, facilitated organic mentorship and career development opportunities

Graduate Student, ECE Department Head Search Committee **Spring 2021**

- Interviewed candidates on ideas and vision, provided feedback and recommendations for hiring
- One of 9 senior graduate students (8 PhD students and myself) selected by faculty to be on the committee

Undergraduate Focus Group Advisor, ECE Department **Spring 2019-present**

- Created and adapted ideas for department-wide changes by interfacing undergrad feedback with faculty

Executive Board, Clark Scholars Leadership Committee **Fall 2018-present**

- Developed group engagement activities to build the small cohort experience and fulfill the scholarship's mission of uniting engineering with entrepreneurship and social impact

Community Service

Family Member (volunteer), Thread Baltimore **Fall 2018-present**

- Wove a network of meaningful, constructive relationships in Baltimore, through a 10-year program involving one-on-one mentoring of a student through his Thread Family

Honors and Awards

The Muly Family Undergraduate Research Award, Whiting School of Engineering Commencement, 2021
Department of Defense Science, Mathematics, and Research for Transformation Scholar, 2019
Johns Hopkins Whiting School of Engineering A. James Clark Scholar, 2017
Potomac Electric Power Company Guiding Light Leadership Scholars Program, 2017

Publications

E. Rong, A. Chiu, C. Bambini, Y. Lin, C. Lu, and S. M. Thon, "New chalcogenide-based hole transport materials for colloidal quantum dot photovoltaics," accepted, 2021 IEEE Photovoltaics Specialists Conference

A. Chiu, **E. Rong**, C. Bambini, Y. Lin, C. Lu, and S. M. Thon, "Sulfur-infused hole transport materials to overcome performance-limiting transport in colloidal quantum dot solar cells," *ACS Energy Lett.,* vol. 5, no. 9, pp. 2897-2904, Aug. 2020, doi: 10.1021/acsenergylett.0c01586.
A. Chiu, C. Bambini, **E. Rong**, Y. Lin, and S. M. Thon, "New hole transport materials via stoichiometry-tuning for colloidal quantum dot solar cells," in *IEEE Photovolt. Spec. Conf.,* Jun. 2020, pp. 1096-1097, doi: 10.1109/PVSC45281.2020.9300891.

Talks and Presentations

Johns Hopkins University Whiting School of Engineering 2021 Design Day Dean's Breakfast, Invited Video. Baltimore, Maryland, May 2021; *New hole transport materials for colloidal quantum dot solar cells.*
Johns Hopkins University Sustainability Leadership Council Symposium, Contributed Talk. Baltimore, Maryland, April 2020; *Engineering new hole extraction materials for colloidal quantum dot solar cells.*
Johns Hopkins University Undergraduate Research Symposium, Contributed Talk. Baltimore, Maryland, October 2019; *Engineering new hole extraction materials for colloidal quantum dot solar cells.*
Johns Hopkins University DREAMS Undergraduate Research Day, Poster. Baltimore, Maryland, April 2018; *Scalable spray-cast deposition of colloidal quantum dot solar cells*